An Investigation into UV Fluorescence in Feldspar Group Minerals

Natasha Morrison

Submitted in Partial Fulfillment of the Requirement for the

Degree of Honours Bachelor of Science,

Department of Earth Sciences

At

Dalhousie University

Halifax, Nova Scotia

March 17th, 2013

Submitted to: Dr. Richard Cox

Dr. Martin Gibling

Distribution License

DalSpace requires agreement to this non-exclusive distribution license before your item can appear on DalSpace.

NON-EXCLUSIVE DISTRIBUTION LICENSE

You (the author(s) or copyright owner) grant to Dalhousie University the non-exclusive right to reproduce and distribute your submission worldwide in any medium.

You agree that Dalhousie University may, without changing the content, reformat the submission for the purpose of preservation.

You also agree that Dalhousie University may keep more than one copy of this submission for purposes of security, back-up and preservation.

You agree that the submission is your original work, and that you have the right to grant the rights contained in this license. You also agree that your submission does not, to the best of your knowledge, infringe upon anyone's copyright.

If the submission contains material for which you do not hold copyright, you agree that you have obtained the unrestricted permission of the copyright owner to grant Dalhousie University the rights required by this license, and that such third-party owned material is clearly identified and acknowledged within the text or content of the submission.

If the submission is based upon work that has been sponsored or supported by an agency or organization other than Dalhousie University, you assert that you have fulfilled any right of review or other obligations required by such contract or agreement.

Dalhousie University will clearly identify your name(s) as the author(s) or owner(s) of the submission, and will not make any alteration to the content of the files that you have submitted.

If you have questions regarding this license please contact the repository manager at dalspace@dal.ca.

Grant the distribution license by signing and dating below.

_____ _____

Name of signatory Date

DALHOUSIE UNIVERSITY
Inspiring Minds

Department of Earth Sciences
Halifax, Nova Scotia
Canada B3H 4R2
(902) 494-2358
FAX (902) 494-6889

DATE: April 22/2014

AUTHOR: Natasha Morrison

TITLE: An Investigation into UV fluorescence in Feldspar Group Minerals

Degree: BSc Convocation: May Year: 2014

Permission is herewith granted to Dalhousie University to circulate and to have copied for non-commercial purposes, at its discretion, the above title upon the request of individuals or institutions.

ABSTRACT

Feldspar group minerals are among the most abundant mineral groups in the Earth's lithosphere and have been documented, studied and analyzed for a wide range of petrologic purposes. The methods used to examine feldspars include cathodoluminescence, petrographic examinations including Michel-Levee compositions, scanning electron microscope and electron microprobe analysis (SEM and EMP), ion microprobe and laser ablation ICP-MS analysis, studies of isotope ratios and X-Ray Diffraction (XRD). As a result the physical properties and paragenesis of feldspars are well understood, however UV fluorescence is one property which has long been described but has not been fully quantified. In this study, the fluorescence of a selected suite of feldspar group minerals was examined to investigate the link between fluorescence and crystal chemistry through determination of major and trace elements. The methods used included petrographic characterization, UV fluorescing imaging and image analysis, electron microprobe analysis, and crystal-structure modeling. Samples from Canada and the United States were used in this study focusing on compositions of the following alkali feldspars: microcline (including amazonite) and orthoclase (including adularia); and plagioclase feldspars (albite, oligoclase, labradorite, bytownite and anorthite). Features such as intercrystalline impurities were also examined. Fluorescence is generally thought to be controlled by activator elements, typically metal cations (Fe^{2+}, Fe^{3+}, Ti and Mn) or REEs. Electrons within these elements become excited by photons at UV wavelengths which cause electron excitation, i.e. a jump to a higher orbital. The de-excitation of this electron then causes a loss in energy that is released as light, at a different wavelength than that the photon which was originally absorbed. In the case of UV fluorescence these emitted photons are visible to the human eye. Integrating results from all of the methods show that different compositions of feldspar fluoresce with similar colors but at strongly variable intensities. Microprobe data, combined with x-ray mapping and UV imaging, showed that there was a significantly higher intensity of fluorescence in K-feldspars, while plagioclase group feldspars have a much lower intensities. Orthoclase and microcline fluoresced very strongly, albite less so, and anorthite showed the lowest fluorescence intensity. However there was a negative correlation between trace element-activator contents and fluorescence intensity. Taking crystal structure into consideration, the unit cell parameters increase in K-feldspar. This along with the monoclinic structure may allow greater photon channeling and thus increases the intensity of fluorescence. Future work employing more sensitive trace-element analysis and UV spectroscopy and XRD are recommended to fully understand the link between fluorescence and crystal chemistry.

Feldspar, Fluorescence, Geochemistry, K-feldspar, Plagioclase, Ultra Violet light

I TABLE OF CONTENTS

II TABLE OF FIGURES

III TABLE OF TABLES

ACKNOWLEDGEMENTS

I would like to offer sincere thanks to my supervisor Richard Cox for his continuous help and guidance throughout this project. Thank you to Dr. Martin Gibling for his valued feedback and grammar corrections throughout the course of writing this thesis. Added thanks to Gordon Brown and Dan Macdonald for their great help with thin section preparation and EMP analysis. Finally, I would like to thank all of my friends for their cherished support and understanding throughout the course of this thesis.

1.0 INTRODUCTION

1.1 General Statement

Feldspar group minerals occur all over the world, being one of the most abundant mineral groups in the earth's lithosphere. They crystallize at high to low temperatures in igneous rocks and grow in felsic to mafic magmas. Feldspar group minerals form the continuous series of crystallization in Bowen's Reaction Series. The series begins with high-temperature, calcium-rich feldspars, anorthite in its purest form. At lower temperatures, the composition evolves to intermediate sodium-rich feldspars (albite) to potassium-rich, felsic, feldspars (orthoclase). These minerals have been documented, studied and analyzed both qualitatively and quantitatively throughout the history of geology. Due to this long history of study, most of the physical properties and paragenesis of feldspars are well understood. However, the ability of feldspars to react to long- or short-wave ultraviolet (UV) light, i.e., fluorescence, has long been documented but not fully quantified. This study will examine UV fluorescence of a selection of feldspar group minerals in order to investigate the link between the crystal chemistry and UV fluorescence of the mineral.

Fluorescence, according to the Oxford Dictionary, is "the visible or invisible radiation produced from certain substances as a result of incident radiation of a shorter wavelength such as x-rays or ultraviolet light". This phenomenon is important because only certain elements can react to the energy and fluoresce, each at their own different wavelength, and thus minerals will fluoresce with different colors. Identifying these minerals and the elements and/or crystal structures which produce corresponding fluorescence can help in identifying element distributions in minerals, including heavy rare earth elements (HREEs) and light rare earth

elements (LREEs). These could be used in finding economic deposits of important minerals and tracing geologic processes.

1.2 Feldspar Minerals

Feldspar group minerals are the most common group of minerals in the Earth's lithosphere. The group itself has over 20 recognized members (Table 1) with these minerals either falling under the Alkali-feldspar or Plagioclase-feldspar subheadings. Feldspars are tectosilicates and have a monoclinic or triclinic symmetry. The three main mineral end members of this group are Anorthite (**Ca**$Al_2Si_2O_8$), Albite (**Na**$AlSi_3O_8$) and Orthoclase (**K**$AlSi_3O_8$) (Fig. 1). Other mineral varieties within the plagioclase sub-group are distinguished by the molar percentage of Albite (Ab) and Anorthite (An). The alkali-feldspar group is more commonly described in terms of textural varieties. In the latter case, these alkali feldspar varieties are controlled largely by the ordering of the tetrahedral Al in the mineral structure, which is in turn controlled by the cooling rate of the host rock. Feldspar minerals can also take trace elements into their structures, which typically reflect the conditions of crystal growth from the host magma. These elements enter the structure in specific bond junctures known as T and M sites (Fig. 2). Some of the chemical substitutions include Mg, Ba, Al, Ga, Fe^{3+}, Si, Ge and P at the T site and Na, K, Rb, NH_4, Fe^{2+}, Ca, Sr, Pb, Ba, Eu^{2+}, and La at the M sites (Smith et al., 1974).

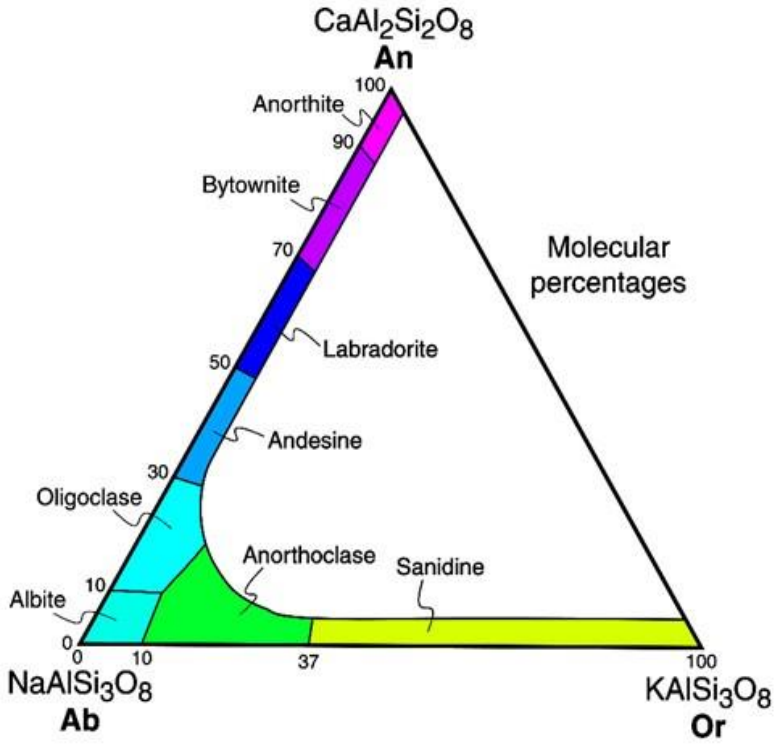

Figure 1: Ternary Diagram of the Feldspar Group minerals showing the three main end members and molecular percentage ranges of others (Elkins et al., 1990).

Albite	$NaAlSi_3O_8$
Amazonite	$KAlSi_3O_8$
Andesine	$(Na,Ca)[Al(Si,Al)Si_2O_8]$
Anorthite	$CaAl_2Si_2O_8$
Anorthoclase	$(Na,K)AlSi_3O_8$
Bytownite	$(Ca,Na)[Al(Al,Si)Si_2O_8]$
Labradorite	$(Ca,Na)[Al(Al,Si)Si_2O_8]$
Microcline	$KAlSi_3O_8$
Oligoclase	$(Na,Ca)[Al(Si,Al)Si_2O_8]$
Orthoclase	$KAlSi_3O_8$
Sanidine	$KAlSi_3O_8$

Table 1: Accepted variations of common feldspar group minerals used in this project and their chemical compositions. Though some of these have the same compositions, variations in crystal structure, trace elements and texture distinguish these from one another (National Audubon Society, 1979).

Crystal structures, as for every mineral, are also very important within the feldspar group. According to Smith and Brown (1974), “the idealized structure of a feldspar is based on the space group C2/m of equivalent general positions (which are potential sites for atoms) and of equivalent symmetry elements which relate them.” Although this is the ideal, variations include C1 and I 2/c structural configurations. These structural configurations, or space groups, are a way of describing how the crystal lattice is configured. Here the C is the lattice where the number is the primary symmetry element. Simply put, the feldspar group minerals have an aluminosilicate framework that follows the general format of MT_4O_8. This framework is made up of linked tetrahedra with large oxygen atoms at the corners and alumina or silicon in the center (T site). The charge is balanced throughout this interlocking tetrahedral framework by placing large atoms in the interstices (M site). These M site atoms are typically sodium, potassium or calcium (Smith et al., 1974). Substitutions among these T and M sites can occur at these sites. The structure can be seen in Figure 2.

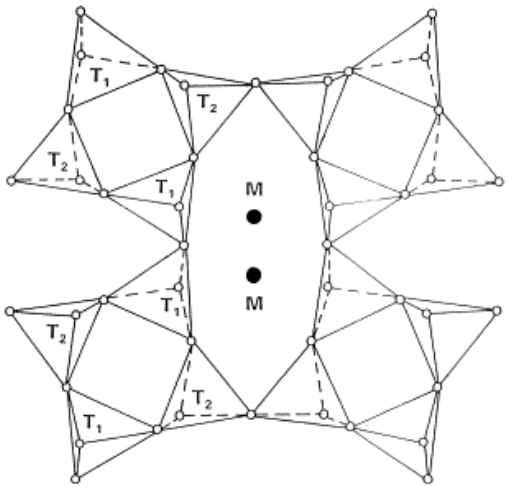

Figure 2: The 4-fold tetrahedron structure of a feldspar showing the T and M sites (Krbetschek et al, 1997).

In thin section, feldspar minerals commonly display a variety of textures, shapes and, less commonly, colors. Twinning in the plagioclase feldspars (multiple), along with some of the alkali

feldspars (simple), is also common. Twinning can include albite twinning (multiple twins) and varieties such as Carlsbad simple twinning or complex crystal lattice effects which produce tartan twinning. The extinction angles of the albite twinning can be used to determine the composition of plagioclases using the Michel-Levy method. Feldspars have first-order birefringence with no pleochroism, meaning that the mineral, in thin section, has double light refraction (in cross polarized light) of 0 to 550 nm along with no change in color in normal, polarized light. There can be two or three cleavage planes within the mineral depending on the variety (Nesse, 2011). However, cleavages are not strongly developed in polished thin sections. More detail of samples will be given in later chapters.

1.3 Thesis Objectives

This thesis will examine the fluorescence of a selected suite of feldspar group minerals and examine the link between fluorescence and crystal chemistry. This will be done through a combination of petrographic descriptions, UV fluorescence and image analysis, electron microprobe analysis, and crystal-structure modeling. The intention is to find a correlation between the crystal chemistry and UV fluorescence or alternatively, a correlation between crystal structure and UV fluorescence. This will be done by looking at the crystal structures, major and trace elements, and any other intrinsic effects. The samples for this experiment have a wide variety of compositions and textures. Although this study focuses on feldspar minerals, similar methods could be applied to other mineral or mineral groups that display UV fluorescence.

2.0 BACKGROUND KNOWLEDGE

2.1 Brief History of Mineral Fluorescence

The first documentation of mineral fluorescence occurred in 1603 when a Bolognian shoemaker named Vincenze Casciarolo discovered that a lapis solaris stone (most likely a barium sulfate) emitted a purplish light in the dark after being baked. It was this occurrence that led Galileo Galilei in 1612 to describe the emission, for which he believed that the light was conceived in the stone and was eventually reborn from it (Barbieri, 2010). Research continued and in 1842 Edmond Becquerel reported that calcium sulfate would emit light when excited by a UV wavelength. He noted that the emission wavelength was longer than that of the incident light (Barbieri, 2010). Until this point the phenomenon was believed to be phosphorescence.

George Gabriel Stokes first looked at mineral fluorescence in a scientific manner in 1852. Stokes was a prolific physicist and mathematician who spent his life studying optical waves and fluid dynamics. In 1852, after studying and publishing papers on polarization and theory of diffraction, Stokes wrote a famous paper on the change in refrangibility of light (Babieri, 2010). Here he described a phenomenon called fluorescence , noting the ability of uranium glass and fluorspar (fluorite) to convert ultraviolet rays, invisible to the human eye, into visible light (Babieri, 2012). From this paper, Stokes developed “Stokes Law of Fluorescence” (Przibram, 1956) in which he deduced that the wavelength of light entering the sample (incident light) must be greater than that of the exciting radiation or emitted fluorescence (Przbram, 1956).

2.2 Mineral Fluorescence

Fluorescence of minerals is not uncommon, occurring in approximately 15% of all known minerals. Within this 15%, only certain variations and compositions of these minerals fluoresce. The fluorescence of these minerals can be observed using ultra violet,- x-ray and cathode light sources. The process by which the fluorescence is produced occurs at an atomic level. Fluorescence (Fig. 3), occurs when fluorescent minerals are introduced to one of the above light sources. The following steps 1 through 4 correspond to the 1, 2, 3, and 4 in Figure 3. (1) The wavelength of light, invisible to the naked eye, excites an electron within the atoms in the crystal structure, and (2) causes it to jump to a higher orbital. Upon de-excitation, (3) the electron loses energy and moves back into the original orbital. (4) This energy is subsequently released in the form of light, at a different wavelength than that absorbed, which, in the case of UV fluorescence, is visible to the human eye. The mineral will fluoresce for as long as it is being exposed to the light source, or in some cases for several seconds afterwards, depending on the amount of energy absorbed (Davidson et al, 2012). Although x-ray and cathode light sources can also be used, this thesis will focus on UV fluorescence.

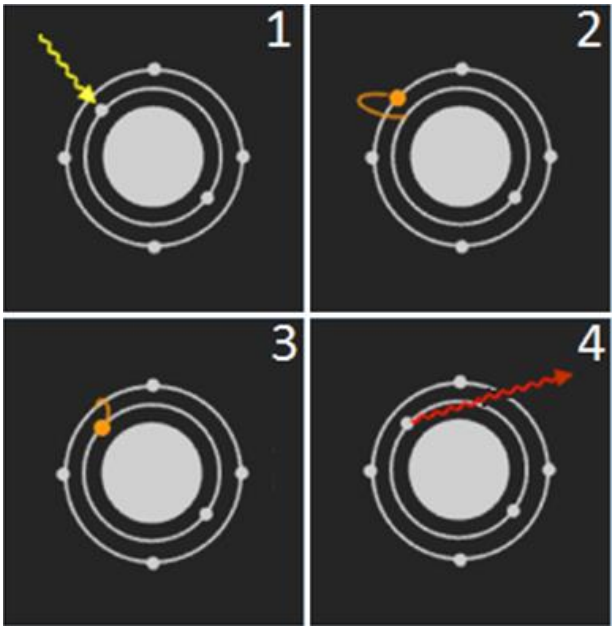

Figure 3: An atomic scale model of the process of fluorescence (modified from Schneider, 2004). See text for explanation of 1-4.

When using ultraviolet light, a wide range of fluorescence can be observed. Most UV lamps have an -ultraviolet light source in long, short and, in special cases, medium wavelengths. These wavelengths correspond to 315-400nm, 100-280nm and 280-315 nm ranges, respectively. These different wavelengths can cause a difference in the fluorescence of the minerals. Most fluorescent minerals are excited by short wavelengths whereas only some produce fluorescence using long wavelengths (Hamblen, 2003). In some cases, like that of mercury-bearing calcite, long- and short-wave energy can cause the calcite to fluoresce pink or blue, respectively (Gaft et al., 2008).

Minerals fluoresce due to intercrystalline impurities known as activators. These activators are characteristically metal cations represented by elements such as chromium, uranium, manganese, tungsten, molybdenum, lead, titanium and boron (Schneider, 2004). A correlation has been determined between fluorescence and rare earth elements including

yttrium, ytterbium, dysprosium and europium, where these activator elements can cause a variation in both the intensity and color of the fluorescence (Schneider, 2004). These activator elements fluoresce due to the atomic process detailed in Fig. 3.

In contrast with activator elements, there are elements that lower or completely remove the mineral's ability to fluoresce. One such effect is that of ferrous iron or copper. These elements can have a dampening effect on fluorescence and can either reduce or completely eliminate the effect of the UV light. These elements are known as quenchers. An over-abundance of activator elements can also have the same effect, though this is not seen in this study (Fluorescent Mineral Society, 2013).

It is not just elemental, crystal chemistry impurities that can cause a mineral to fluoresce. There are certain minerals labeled "self-activated" minerals that fluoresce in their pure state, without the presence of activators. A well-known self-activating mineral is scheelite (Fluorescent Mineral Society, 2013). Other possible sources of fluorescence are the presence of organic impurities or defects in crystal structure. These defects cause a change in the crystal lattice and bond lengths within the mineral and have been hypothesized to lead to mineral fluorescence (Schneider, 2004).

In summary, the presence and variation of activators, quenchers, and crystal structure effects can cause a wide variety of fluorescence in minerals. Although most minerals only fluoresce with a single color per sample, there are cases when multiple colors can be seen at the same wavelength. This is due to zonation during crystal growth or compositional banding of a rock. This mineral zonation can include trace elements, both activators and quenchers,

leading to a color variation during fluorescence. These changes in composition and their effects can be seen in Figure 4. It is also important to note that not all samples of the same mineral will fluoresce with the same color. The presence of different activator minerals will affect the color of the emitted light. For example, minerals containing the uranyl ion (derived from uranium) will fluoresce a yellow-green color due to the overpowering nature of the ion. In the case of scheelite, in the presence of tungsten it will fluoresce its characteristic bright blue color. If molybdenum is included in the crystal chemistry, the color will change to a whitish yellow (Fluorescent Mineral Society, 2013).

Figure 4: Zoned and banded minerals under UV light fluorescing and different wavelengths (Schneider, 2004).

2.3 Fluorescence in Feldspars

Previous research studying the fluorescence of feldspars has been limited. Since the discovery of fluorescent minerals, it has only been noted that feldspars fluoresce and there is little research into the nature of this effect. Modreski (1987) stated that potassium feldspar and albite tend to fluoresce in various shades of red, with variable intensity. He attributed the UV fluorescence to the presence of Fe^{3+}, REEs, Pb^{2+} and other metal activators. Furthermore, the Fluorescent Mineral Society has shown multiple pictures of different feldspar minerals fluorescing, but spectral analysis or other quantification of the effects are sparse. This thesis aims to build on this research and provide analysis of fluorescent feldspar minerals.

3.0 METHODS

3.1 Data Collection

The data for this project were collected using four different methods. Petrographic descriptions, UV imaging and image analysis, electron microprobe analysis, and crystal structure modeling were all used in the collection process. Each method provided unique data, that when combined, allowed conclusions to be reached. The following is an in-depth account of each of these methods, focusing on how they work and how they were used within the context of this project.

3.1.1 Petrographic Description

Of the sixteen samples used in this project, eight were cut into thin sections. These sections were examined under a Nikon 50i transmitted-light microscope in both cross-polarized and plane-polarized light. Each thin section was examined for textures, inclusions, reaction rims and signs of twinning. A sketch and full description was completed for each section. These sections were then exposed to long wave UV light and photographed under 10x optical zoom with a Nikon Eclipse camera (50i Pol, LV-UEP1).

3.1.2 Electron Microprobe

An electron microprobe allows for the characterization and observation of heterogeneous materials on a nano- to micro-meter scale. It works by irradiating a polished section with a finely focused electron beam. This beam, containing accelerated particles, can be used in one of two ways. Firstly, it can be used as a single, static point for point quantitative and qualitative analysis. Secondly, it can be used to image the entire section by rastering the beam across the entire sample. The interaction created by focusing this electron beam on the section

creates different types of signals. These signals are dependent on the strength of the electron beam being emitted and can be used for secondary electron imaging, backscattered electron imaging, and x-ray characterization (Goldstein et al., 2003).

In quantitative (and some qualitative) analysis, these signals are emitted as different wavelengths of x-rays. These x-rays are, as previously stated, emitted by the interaction between the accelerated particles in the electron beam and the carbon-coated polished section. These x-rays are then captured by one of the five spectrophotometers on the machine and the elemental composition of that point or area is recorded (Goldstein et al., 2003).

Electron microprobe work was completed using a JEOL 8200 Superprobe using carbon-coated, polished thin sections. Each polished section had key points marked. These key points represented (i) the common (bulk) texture of the mineral, (ii) exsolutions, and (iii) reaction rims present within the section. Each section was set under the probe and these key areas were marked. A full chemical composition was given for each sample point including dominant major and selected trace elements. The major and minor elements included Si, Ca, K, Na, Al, Mn, Ti, Ba Fe, Pb and Sr. These elements distributions were examined for ties to the observed fluorescence. It is important to note that in analyzing for these elements, the microprobe records them in terms of oxide percent.

Once these analyses were completed, an average element weight percent, normalized to 100, was calculated for each group. Using conversion factors to calculate weight percent from percent oxide the original analyses were converted, the remaining percentage (out of 100) calculated to be the percent oxygen. These calculations were then manually entered into the

microprobe for the given mineral, and the analysis was re-run to analyze for rare earth elements (RRE's). This was done to increase probe sensitivity by only analyzing the RRE's and not reanalyzing for already known elements. These elements included La, Ce, Pr, Nd, Sm, Eu, Gd, Dy, and Y.

X-ray mapping was also done using the electron microprobe. This provided images of the elemental distribution throughout the sample. These maps were used to point out variations within the minerals and determine the elements responsible for the variation. These elements were documented for further use in crystal structure modeling. The maps also analyzed for Si, Ca, K, Na, Al, Mn, Ti, Ba, Fe, Pb, and Sr.

3.1.3 UV Imaging and Image Analysis

The photos referenced in 3.1.1 were taken under short-wave UV light with a 15 second exposure. These pictures were then imported to *ImageJ*. Using the *ImageJ* software, a relative intensity was able to be calculated using the method outlined in Burgess et al., 2010. This method uses pictures, preferably that of fluorescing images of the same exposure. These images are then changed to greyscale, and the intensity of the greyscale is then measured for the fluorescing area, and then the background. The average intensity of a pixel is then equivalent to that of the relative intensity of the mineral.

3.1.4 Crystal Structure Modeling

Crystalmaker is a computer program that creates crystals in a digital, three-dimensional format using crystal structures, elements, the relative atomic radii, bond lengths and other features. For this project, a synthetic crystal lattice of the main end-members of the feldspar group were created using the lattice parameters laid out in Nesse (2011). *Crystaldiffract* is

another part of this program suite which generates synthetic powder x-ray diffraction data from the modeled crystal structures. These data change with each change of the crystal structure. An attempt was made to find a pattern between crystal structure (i.e. unit cell parameters), the activator elements present and fluorescence.

3.2 Data Analysis

Using the methods explained above, a large amount of data was produced. Each of the results from the methods were analyzed individually then put together to form conclusions. Firstly, the petrographic description allowed the identification of features within the mineral including inclusions, reactions and textures such as twinning. This characterization allowed for the identification of the main feldspar types and features present.

The UV image analysis was then done using the *ImageJ* software. With the relative intensity calculations, a correlation with the probe data was made. This was done by plotting the relative intensities against the total LREE wt% and the Ca, Na, and K-feldspar end member. These end members were calculated using wt% oxides. For example, the Ca was calculated using the equation Ca = CaO/(CaO+NaO+K_2O). These plots were then analyzed for correlations (both positive and negative), between the relative intensities and the wt % or end member calculations.

The probe data, both major and minor elements, along with the rare earth elements, were then analyzed. The first probe analysis, the major and minor elements, was used to determine the composition of the samples. This was done by normalizing the data to calculate the percent albite (Ab), anorthite (An) and orthoclase (Or). These end-member percentages

were then plotted on ternary diagrams to determine their feldspar classification. The REE data was used in the UV image analysis described above.

Following this, the synthetic XRD data were analyzed. Each peak of the obtained graphs was analyzed to obtain the unit cell parameters along with the D spacing values. Correlations between the changes in the unit cell parameters (therefore changes in the composition) were then correlated against the relative intensity of the minerals fluorescence.

The microprobe data, as well as the x-ray mapping, were then used to seek a correlation between the elemental compositions of the mineral and the fluorescence. Elemental anomalies in each sample were referenced against the spectra to see if specific elements were causing fluorescence at specific wave-lengths. Together with the crystal structure and petrographic data an overall conclusion was formed.

3.3 Sources of Error

Aside from the expected human and calculation sources of error, it is important to note the additional microprobe error. During the use of the probe, the display monitor in which to focus the beam onto the thin section was out of commission. In its absence, two focusing methods were used. For the x-ray maps the beam was focused using the spectrometer. Here the silica peaks were adjusted to their highest possible point, so that the beam was as focused as it could be. For the quantitative analysis, each point was focused by looking into the apparatus and focusing the crosshairs by sight. Neither of these methods was as reliable as the automatic focus with the monitor, thus yielding some less reliable element totals in the 96 -97

wt% range. Although not ideal, these data proved to be accurate for examining differences between the various feldspar varieties and were more than sufficient to complete this thesis.

4.0 RESULTS

4.1 General Statement

The data collected yielded very promising results throughout these experiments. Though sixteen samples were originally chosen, due to size and quality of the samples, only eight were chosen to be cut into thin and polished sections. Of these eight samples, there was a wide range of feldspar group varieties, from orthoclase, through to albite, ending with anorthite. These samples included whole rock samples vs single mineral specimens. This included a dacite, granite and a diorite with plagioclase crystals, along with whole mineral samples of orthoclase, andesine, labradorite, microcline, and a presumed amazonite. It is interesting to note that the eighth sample, the amazonite, was discovered to be a green, possible chloro-, apatite after an Energy Dispersive Spectometry (EDS) scan. Thus, in the absence of mineral analysis, historical descriptions of UV fluorescence must be treated with caution.

4.2 Whole Sample Analysis

The initial analysis consisted of simply noting which of the feldspar group minerals fluoresced and which did not. It was evident that most of the feldspar group minerals fluoresced, to some degree. However, the intensity with which they fluoresced varied dramatically through the minerals. All sixteen minerals were photographed both in plane (incident) and shortwave ultraviolet light. The seven main samples can be seen in Figure 5.

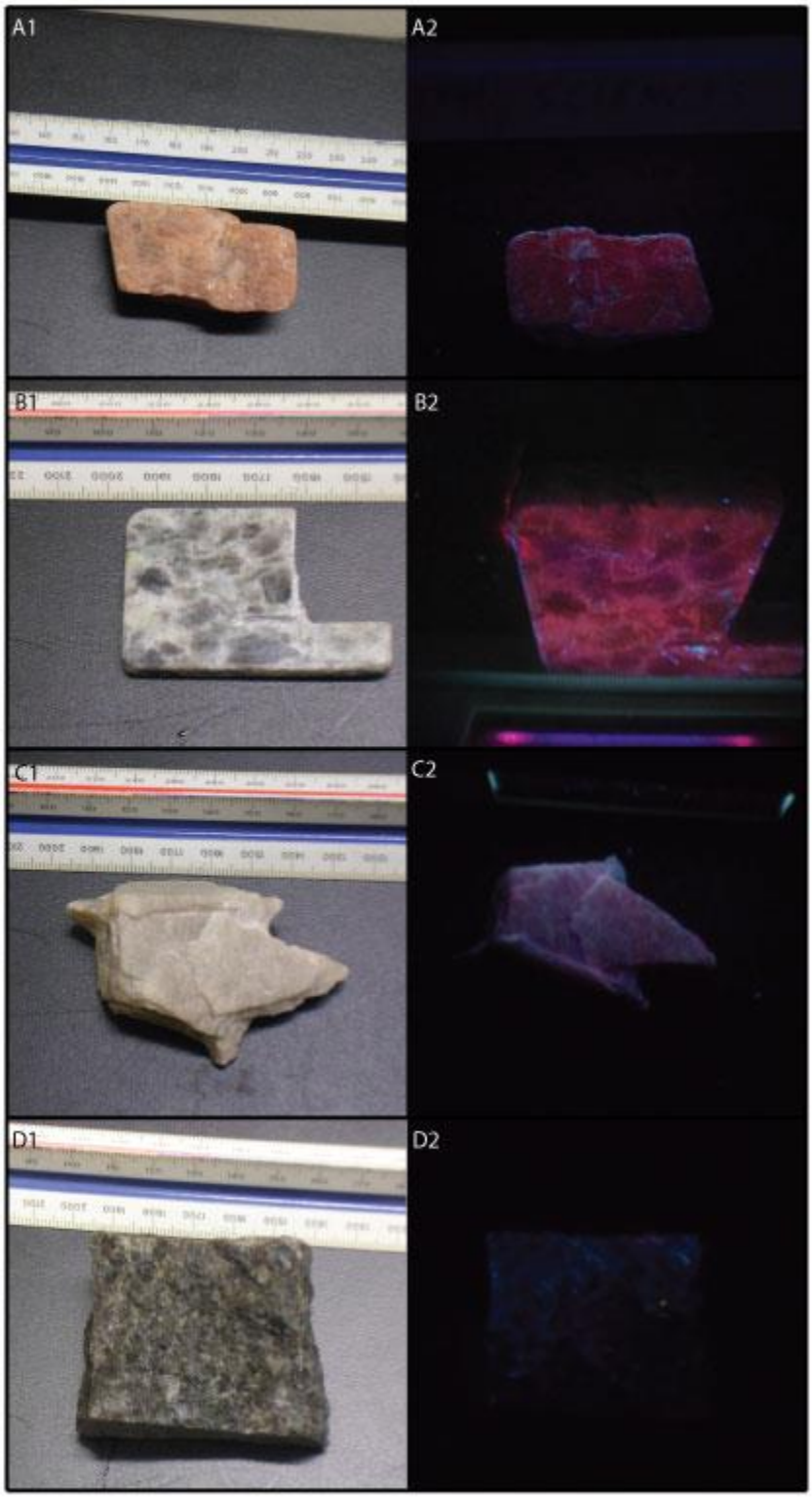
A1
A2
B1
B2
C1
C2
D1
D2

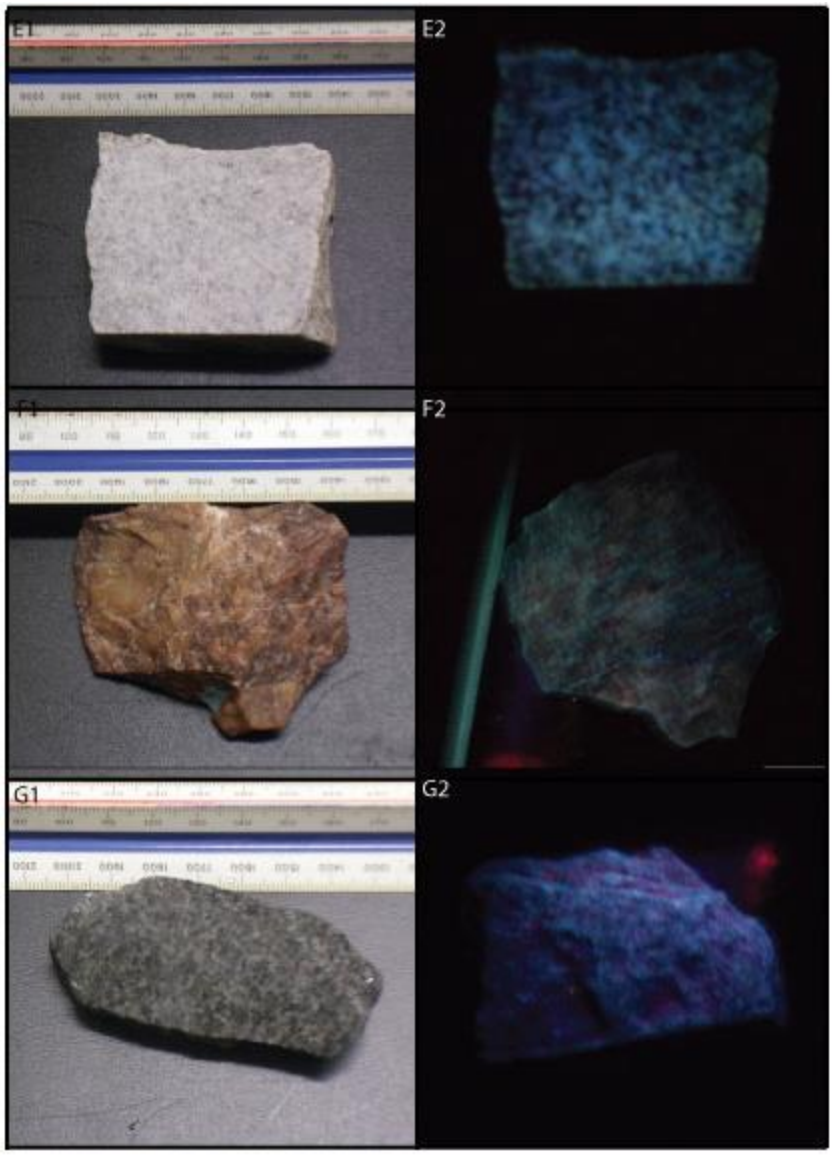

Figure 5: Photographs of the samples in 1-plain and 2-UV light to show whole light fluorescence. The samples are labeled as followed: A) orthoclase B) bytownite C) microcline D) labradorite E) granite F) dacite G) diorite. These were the seven samples used in thin section analysis.

It is evident from the above photos that most, to at least some degree, fluoresce. Some, however, are simply reflecting the UV light off of their polished faces (seen in the reflection of the exact same color as that of the light). The fluorescence for all samples has a red or pink shade to it, apparently emitting light in the red wavelength. This wavelength is between 640 and 720 nm. The orthoclase, bytownite, microcline and diorite all show strong, pink

fluorescence. The labradorite, granite, and dacite, however, do not show strong fluorescence, if they show any at all. What color they do show is mostly a contribution from the reflection and scattering of the UV light off the vitreous minerals.

4.3 Petrographic Description

The seven thin sections were fully described. Within these descriptions, textures, inclusions or exsolution lamellae and mineralogy were all noted. Optical figures were also taken for each of the samples. Furthermore, photomicrographs of these sections exposed to UV light were taken and the UV light's effects were described. In looking at the fluorescence photos, a comparison with the texture or minerals corresponding to different intensities of fluorescence was made. The comparison of the PPL versus the fluorescing images are in the same optical zoom although not necessarily the same field of view. A summary of the findings can be found in Appendix A.

4.3.1 Sample 303

Sample 303 is orthoclase with an unknown origin (Fig. 6A). Brownish-orange in hand sample, it is colorless to light brown in thin section with a low relief and no pleochroism. With large euhedral to subhedral crystals, the sample has uneven fracturing with what looks to be 90° cleavage in some areas.

In cross-polarized light, it was evident that there was a perthitic texture throughout the sample. Exsolution lamellae of albite ran throughout the orthoclase. The orthoclase has a low, first-order birefringence (maximum ~ 0.005) with some small oxide inclusions throughout the mineral. Finally, it has a biaxial negative optical figure with a 2V angle of ~71°.

This sample was one of the most promising samples for fluorescence. In hand sample, the orthoclase fluoresces an intense, bright pink color. This pink color can be seen in thin section as well. The orthoclase in this case fluoresces the bright, pink color while the perthitic exsolutions fluoresce dimly, if at all (Fig. 6B).

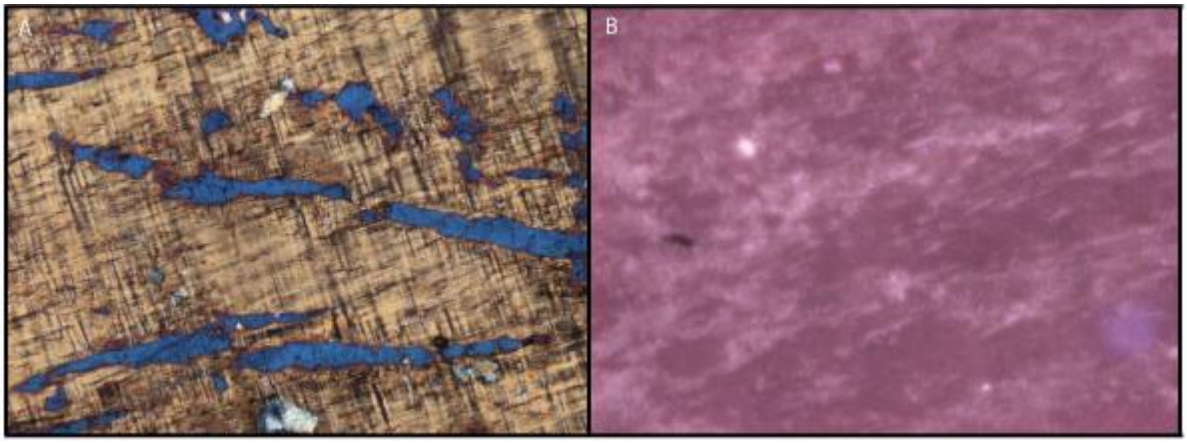

Figure 6: A) Orthoclase viewed in XPL and 10X zoom. This shows the perthitic exsolutions, tartan twinning and oxide inclusions. B) The sample (not same orientation) under ultra violet light. The pinkish/purple color is the fluorescence while the white is a reflection of the light (i.e. not fluorescing).

4.3.2 Sample 414

Sample 414 was labeled as a gabbro. The hand sample was light to dark grey in color and fluoresced a light pink color in some areas. It has some conchoidal fracturing with two cleavages. In thin section, the rock contains a small amount of quartz, oxides, a small amount of muscovite and approximately 90% plagioclase (approximately 35 to 40% anorthite). The sample also contains an amount of biotite. This would classify the sample as a diorite. The plagioclase has a low relief, and is colorless with no pleochroism.

In cross-polarized light, zoning could be seen in many of the crystals. Using the Michel-Levy method, this plagioclase had an average percent Anorthite of 45. This classifies the

plagioclase as an andesine. Some simple twinning was also visible (Fig. 7A). This first-order birefringant andesine has a biaxial positive optical figure with a 2V angle of approximately 75°.

This particular sample was interesting when exposed to UV light. Many of the crystals in the hand sample seemed to fluoresce, and the same was seen in the thin section. The feldspar group minerals (the andesine and potassium feldspar) fluoresced a light pink color. Variation in fluorescence can be seen within the zoned crystal in Figure 7B. This is described in greater detail by the x-ray maps.

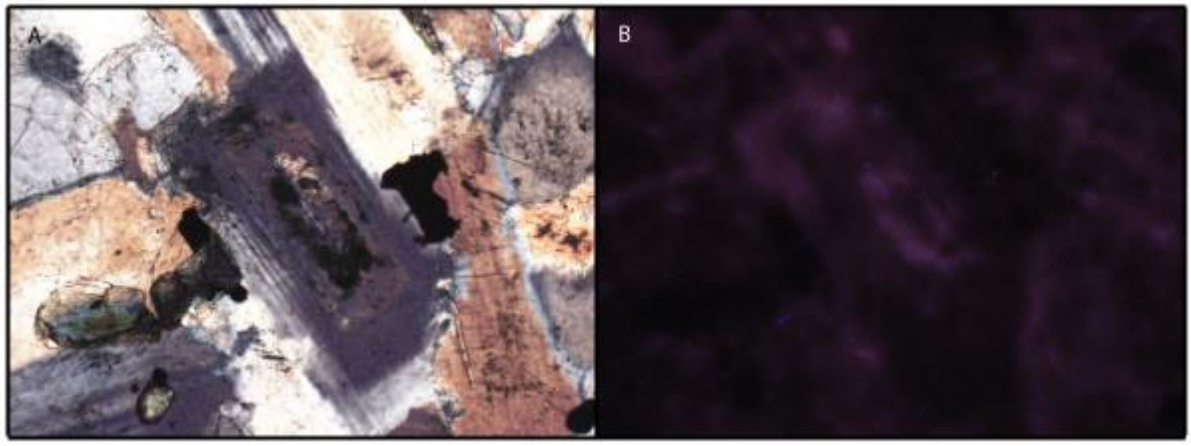

Figure 7: A) The zoned andesine in XPL and 20X optical zoom. This is surrounded by muscovite, oligoclase and k-feldspar. B) The same image, with the sample exposed to UV light. Note the variations in fluorescing intensity within the zoned minerals.

4.3.3 Sample 446

Sample 446 is a dacite from Montana. The hand sample is light brown to a darker greyish brown, equigranular, and massive. In the thin section, hornblende, plagioclase, quartz and biotite were visible, and oxide minerals were present throughout the sample. The plagioclase has low relief compared to the higher relief groundmass. It exhibits no pleochroism and is colorless in thin section.

In cross-polarized light, Carlsbad twinning was evident. The crystals also had a low, first-order birefringence with a maximum of approximately 0.008. These subhedral crystals have a biaxial positive optical figure with an approximate 2V angle of 78°. Using the Michel-Levy method the plagioclase was identified as an andesine.

When exposed to UV light, the entire sample emitted very low intensity fluorescence. In thin section, the result was much the same. The ground-mass and surrounding minerals did not show fluorescence. The andesine however fluoresced at a low intensity.

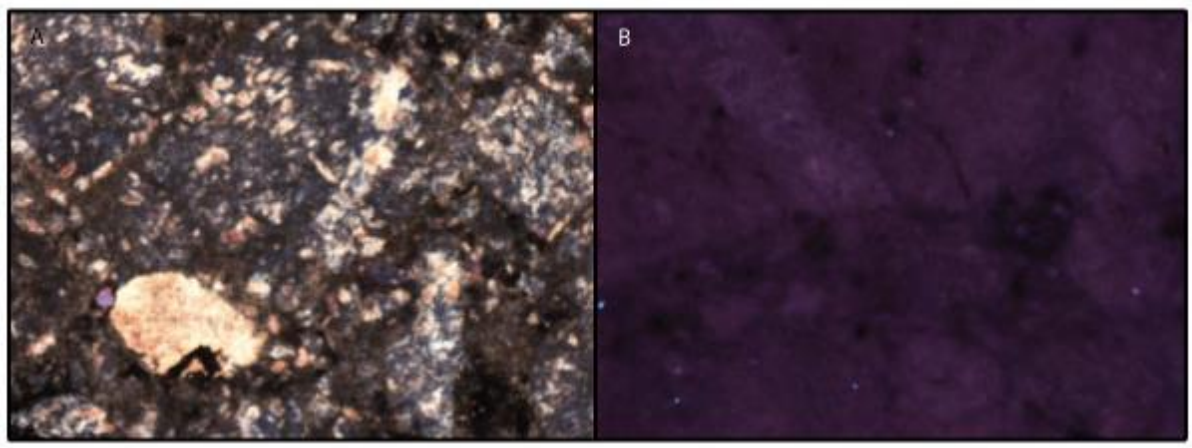

Figure 8: A) The dacite sample showing plagioclase, hornblende, pyroxene and biotite. This is shown in 10X optical zoom and XPL. B) The dacite when exposed to UV light. The sample as a whole fluoresces with a very low intensity, although the plagioclase seems to have a slightly higher intensity.

4.3.4 Sample TMB

Sample VIII-11-1 was labeled in the collection as an anorthite from Ten Mile Bay, Labrador. In hand sample, the rock contains white to grey visible grains with an approximate medium density (heaviness). Further inspection under a microscope showed the mineral was 55-66% anorthite meaning it is actually a labradorite. The thin section contained 95% labradorite and 5% actinolite. Trace amounts of magnetite are also present.

This labradorite is light brown to colorless in thin section, with a medium relief and no sign of pleochroism. These tabular, euhedral crystals have three, perfect 90° cleavages and some uneven fracturing throughout. In cross-polarized light the sample has first-order, low birefringence with a maximum value of approximately 0.01. It has significant Carlsbad twinning with an extinction angle of 45°. In looking at its optical figure, the bytownite has a 2V angle of approximately 84° and is biaxial positive.

This sample was interesting when exposed to UV light. The hand sample as a whole seemed to fluoresce a pink color. When looking at it in thin section, the mineral itself did not seem to fluoresce at all. There were small, flame structures (i.e. micro-inclusions) that seemed to be fluorescing intensely in the pink color range. These micro-inclusions were marked for further microprobe analysis.

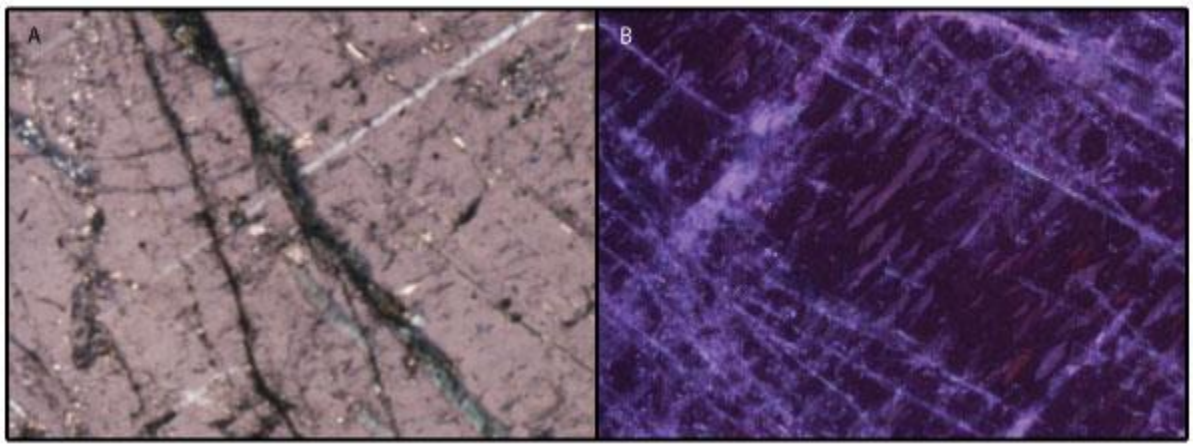

Figure 9: A) The Ten Mile Bay labradorite in XPL and 10X optical zoom. The body of the mineral can be seen as well as fractures and micro-inclusions. B) 10X optical zoom as well as exposure to UV light. The micro-inclusions are fluorescing at a much higher intensity than the host mineral.

4.3.5 Sample VIII-11-1

This sample is a labradorite from Tabor Island, Labrador. In hand sample the labradorite is dark in color, with a medium to high density with labradorescence. In thin section the sample is a greyish/brown color with medium relief and with no pleochroism. Most of the grains were tabular and euhedral with a few anhedral, rounded crystals. These crystals have uneven fracturing with a 90° cleavage in some areas. In plane-polarized light green reaction rims can be seen around oxide inclusions as well as inclusions of clinopyroxene.

In cross-polarized light the sample has a low, first-order birefringence with a maximum of 0.01 along with an extinction angle of 55°. The mineral has Carlsbad twinning with oxide exsolutions in certain areas. With a 65% anorthite value, this labradorite has a biaxial positive optic figure with a 2V angle of 88°.

This labradorite was not a very fluorescent sample overall, in hand sample or thin section. Looking at the thin section when fluorescing, the mineral seems to be fluorescing a very dull pink. The intensity ranges from non-existent to very dull. This contributes to the non-fluorescing nature of the entire hand sample.

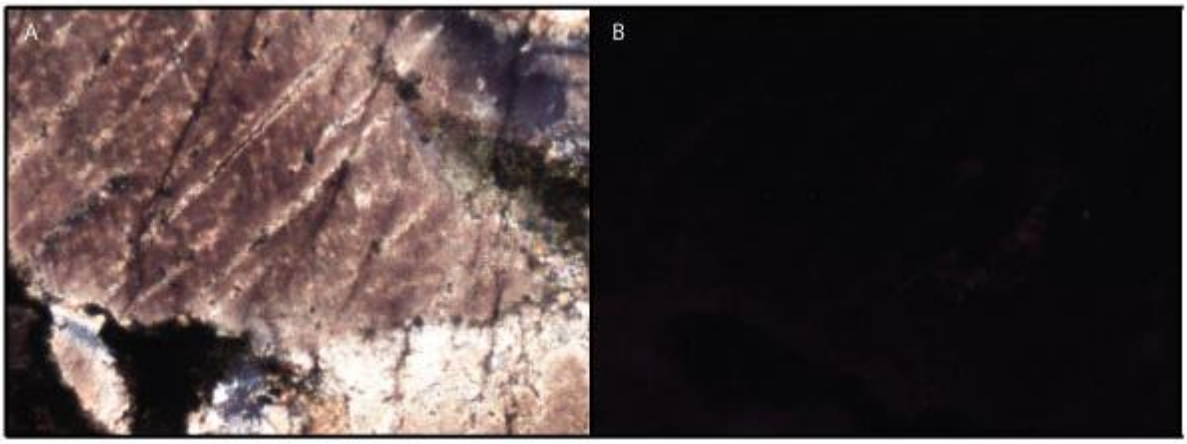

Figure 10: A) A large labradorite crystal in XPL and 10X optical zoom. Reaction rims and pyroxene can be seen in the left-hand corner of the image. B) The same image exposed to UV light. There is a low intensity fluorescence coming from the labradorite while no fluorescence is coming from the pyroxene or reaction rims.

4.3.6 Sample VIII-7-4

Sample VIII-7-4 is a microcline from Hackberry, Arizona. In hand sample, the mineral is light grey to white in color and has a low density. Looking at the thin section in plane-polarized light, the sample was colorless with a low relief. The crystals are elongate (parallel) with some uneven fracturing and two perfect 90° cleavages. Within the whole thin section there is approximately 90% microcline with the final 10% being made up by brown, high-relief inclusions of albite.

In cross-polarized light, the microcline has low, first-order birefringence with a maximum of 0.007 and an extinction angle of 41°. Tartan and Carlsbad twinning can be seen throughout this sample in addition to very few spots with perthitic exsolution lamellae. In looking at the optical figure, the microcline had a 2V angle of ~68° with a biaxial negative figure.

The microcline fluoresced in the presence of UV light but was relatively dim. The inclusions of albite throughout the sample did not seem to fluoresce, or fluoresced very dimly.

The body of the mineral also dimly fluoresced at a darker shade of pink (purple). This microcline was less fluorescent that the other K-feldspar (orthoclase) sample.

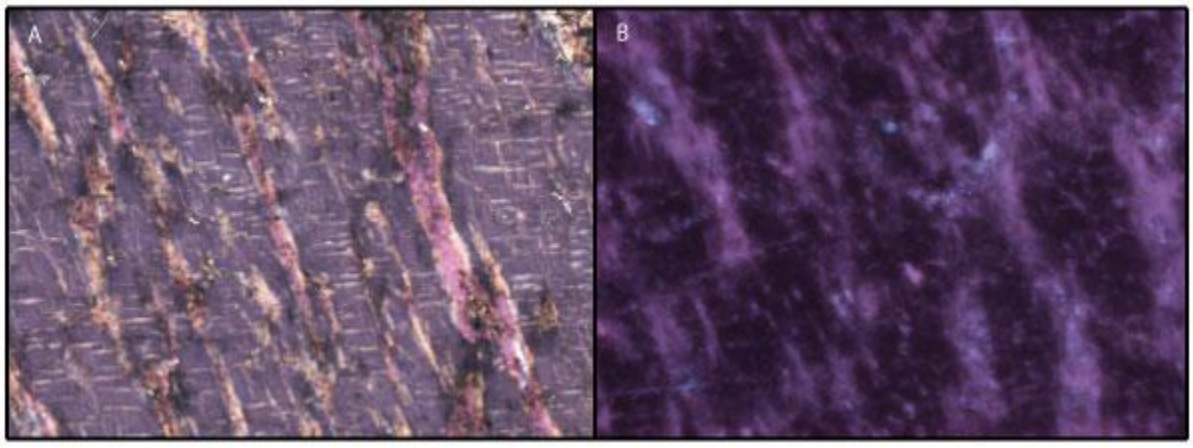

Figure 11: A) The microcline sample in XPL and 10X optical zoom. It shows the host microcline, tartan twinning and inclusions of albite. B) The microcline under UV light. This shows a deeply fluorescing microcline with a much dimmer albite throughout.

4.3.7 Sample VIII-9-2

Sample VIII-9-2 is a white to gray, fine-grained granite. Of an unknown locality and intrusive, igneous origin the hand sample is dense with clear evidence of biotite, muscovite, plagioclase and quartz. Taking a closer look, the mineralogy and percentages of this mineral are as follows: approximately 40% plagioclase, 45% quartz, 10% muscovite, 5% muscovite, and small traces of K-feldspar. The plagioclase component has a range of 19 to 23% Anorthite making it oligoclase.

This oligoclase has no pleochroism, low relief, and first-order birefringence in cross-polars. These grains were subhedral to anhedral with two perfect cleavages and an uneven fracture. These grains have simple twinning, as well as some the occasional periclase twinning. Based on the optical figure, the grains had an average 2V angle of 83°and a biaxial positive figure.

The section, under ultra violet light, did not seem to fluoresce very much. Although the oligoclase did fluoresce, it was at a very low intensity, with a light pinkish color. The grain boundaries within the section also seem to have low-intensity fluorescence.

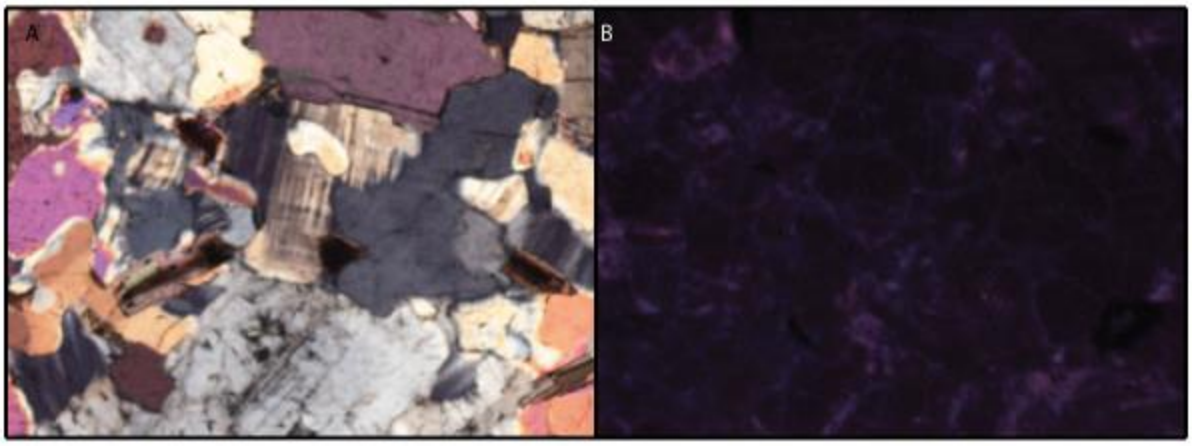

Figure 12: A) A twinned oligoclase crystal with biotite, muscovite, other oligoclase crystals and quartz in XPL and 10X optical zoom. B) Granite sample exposed to UV light. The oligoclase can be seen dimly fluorescing.

4.4 UV Relative Intensity and Image Analysis

The image analysis was completed using the photomicrographs of the fluorescing minerals, along with the *ImageJ* software. The analysis yielded relative intensities from approximately 13 to 110. These intensities were plotted as a line graph. This line graph was then plotted against a histogram of the calculated total LREE's and percent end-members of Ca, Na, and K (Table 2). This then showed a correlation, or anti-correlation, of the relative intensity versus the minerals. The below histograms are labeled one through six, representing (1) Sample VIII-11-1, (2) Sample TMB Body, (3) Sample 414, (4) Sample TMB Inclusions, (5) Sample VIII-7-4, and (6) Sample 303. The samples were ordered from lowest to highest relative intensity. The complete REE probe data can be seen in Appendix B.

	LREE	Ca End-Member	Na End-Member	K End-Member	Fe	Pb	Calculated Intensity	StDev of Calculated Intensity
Labradorite	0.118	0.718	0.260	0.021	0.225	0.049	13.095	5.22
Ten Mile Bay Body	0.095	0.633	0.343	0.024	0.200	0.037	39.028	1.78
Ten Mile Bay Inc	0.041	0.005	0.033	0.962	0.046	0.037	72.134	2.14
Diorite	0.084	0.548	0.431	0.020	0.109	0.034	49.585	3.18
Microcline	0.108	0.001	0.034	0.965	0.024	0.006	79.802	3.78
Orthoclase Body	0.083	0.001	0.057	0.942	0.033	0.046	107.864	1.59

Table 2: Calculated relative intensity values, total LRRE of the samples and calculated percent end-members of the five given samples.

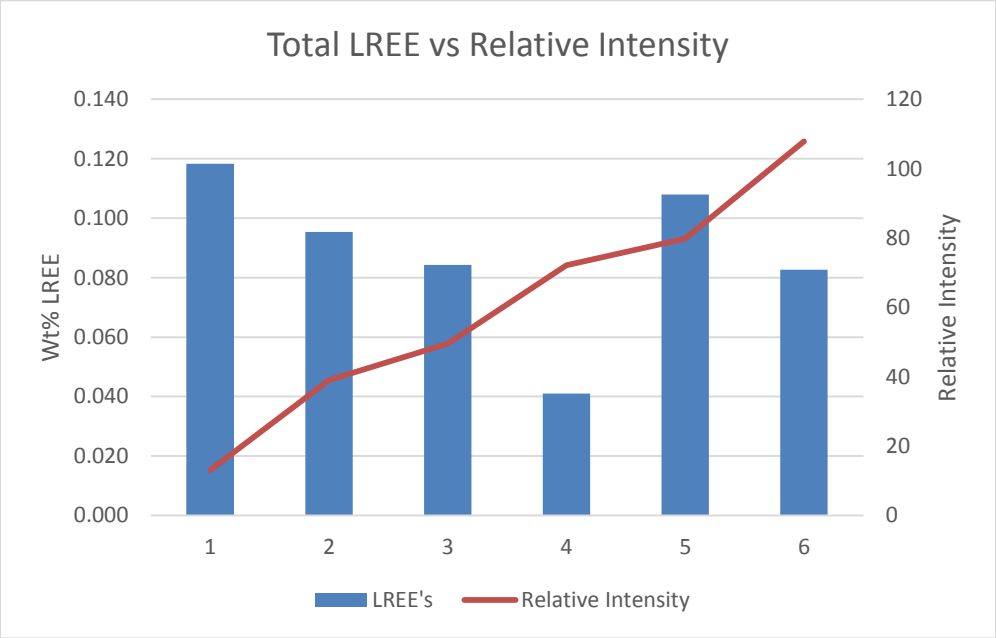

Figure 13: Total Light REE plotted in the blue histograms versus the relative intensity of the six samples plotted as a line graph. (1) Sample VIII-11-1, (2) Sample TMB Body, (3) Sample 414, (4) Sample TMB Inclusions, (5) Sample VIII-7-4, and (6) Sample 303.

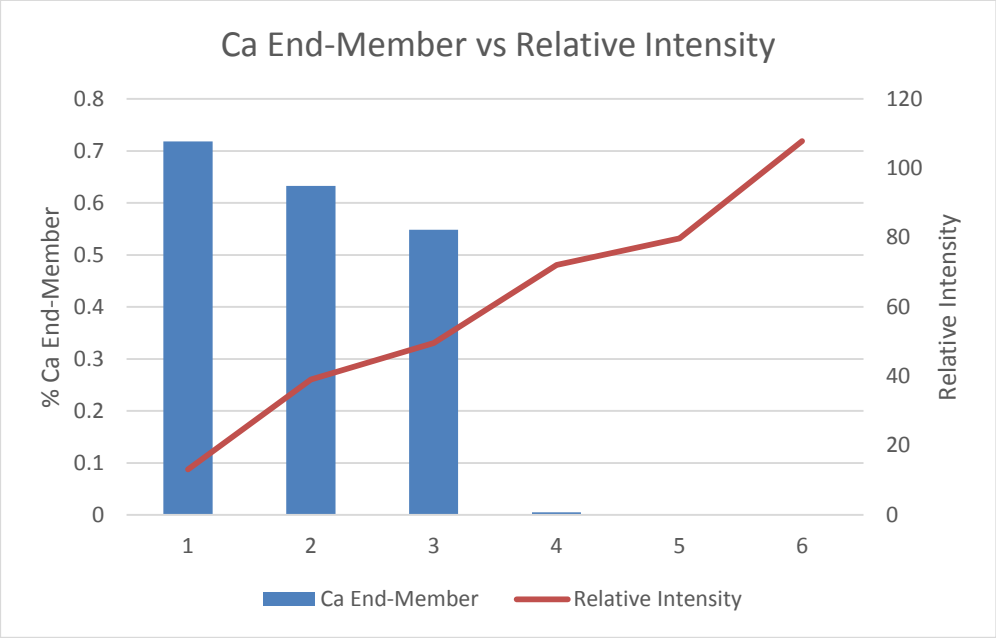

Figure 14: Percent of Ca end-member plotted in the blue histograms versus the relative intensity of the six samples plotted as a line graph. (1) Sample VIII-11-1, (2) Sample TMB Body, (3) Sample 414, (4) Sample TMB Inclusions, (5) Sample VIII-7-4, and (6) Sample 303.

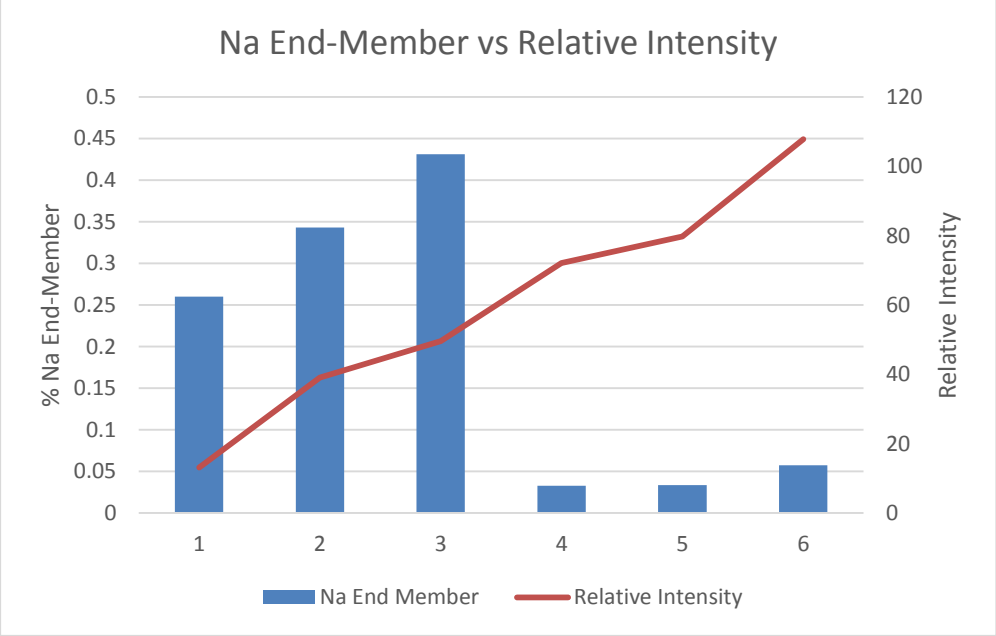

Figure 15: Percent Na end-member plotted in the blue histograms versus the relative intensity of the six samples plotted as a line graph. (1) Sample VIII-11-1, (2) Sample TMB Body, (3) Sample 414, (4) Sample TMB Inclusions, (5) Sample VIII-7-4, and (6) Sample 303.

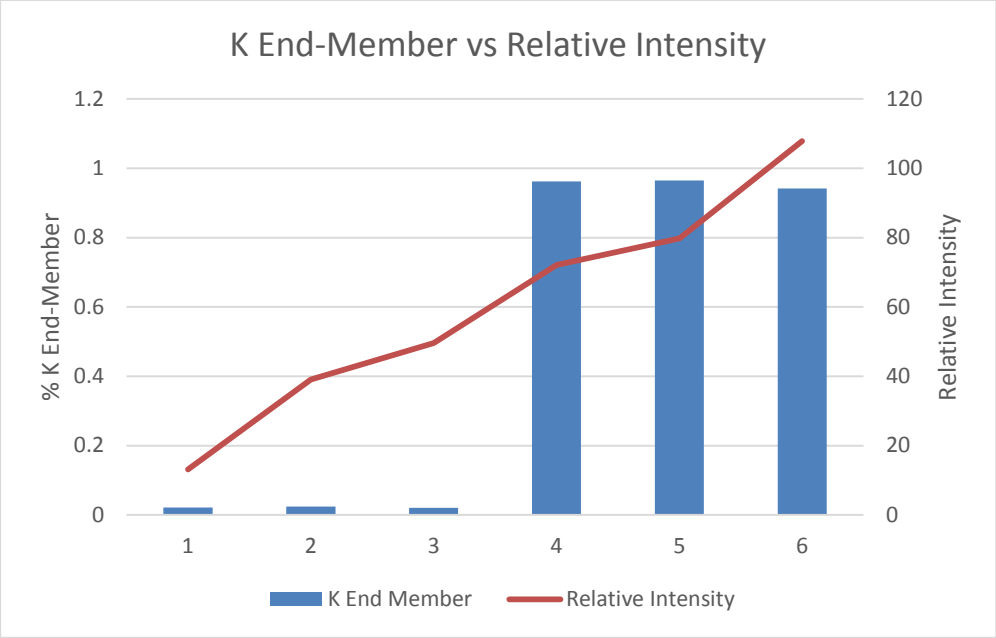

Figure 16: Percent K end-member plotted in the blue histograms versus the relative intensity of the six samples plotted as a line graph. (1) Sample VIII-11-1, (2) Sample TMB Body, (3) Sample 414, (4) Sample TMB Inclusions, (5) Sample VIII-7-4, and (6) Sample 303.

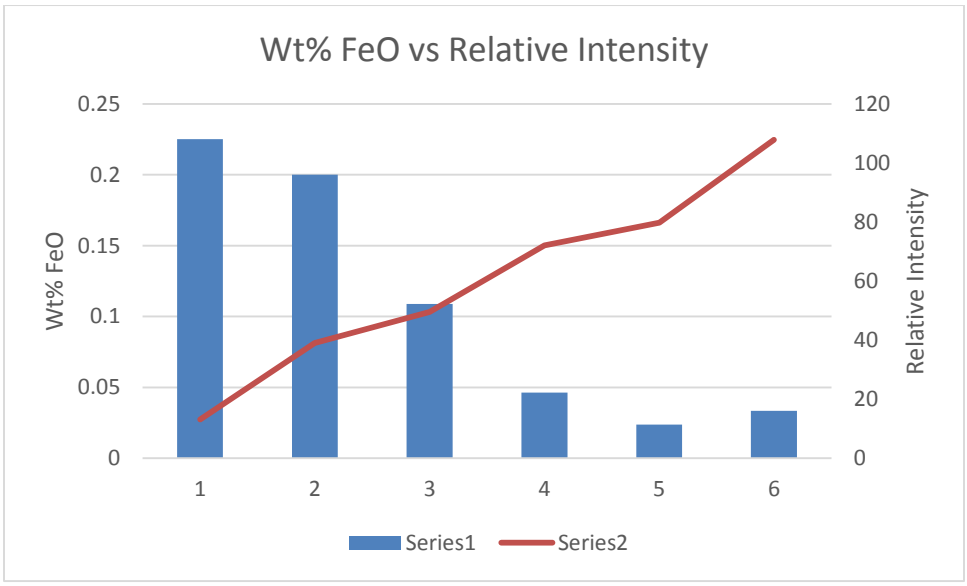

Figure 17: Wt% FeO plotted in the blue histograms versus the relative intensity of the six samples plotted as a line graph. (1) Sample VIII-11-1, (2) Sample TMB Body, (3) Sample 414, (4) Sample TMB Inclusions, (5) Sample VIII-7-4, and (6) Sample 303.

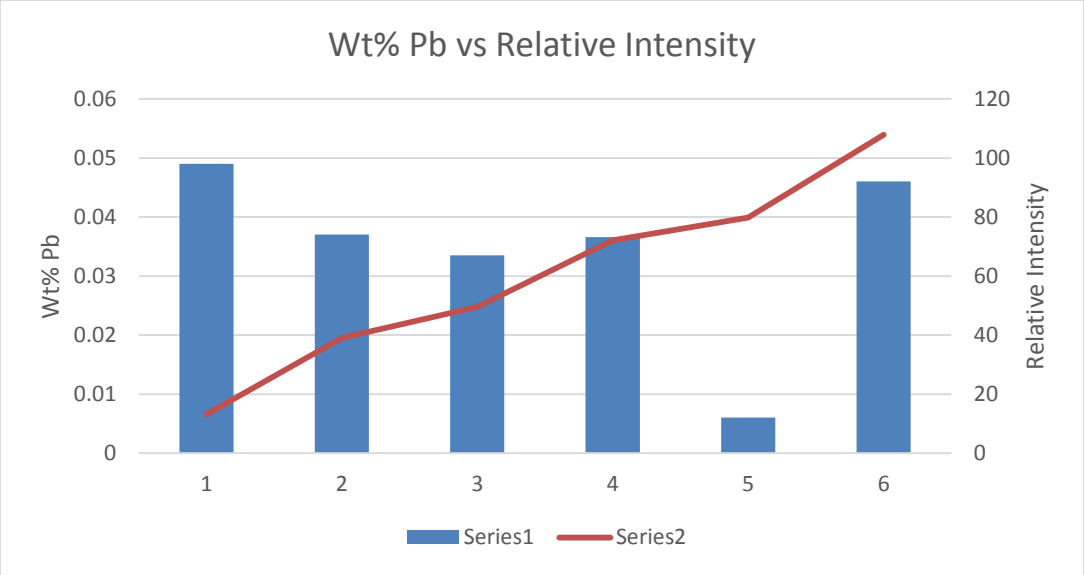

Figure 18: Wt% PbO plotted in the blue histograms versus the relative intensity of the six samples plotted as a line graph. (1) Sample VIII-11-1, (2) Sample TMB Body, (3) Sample 414, (4) Sample TMB Inclusions, (5) Sample VIII-7-4, and (6) Sample 303.

The plots showed interesting relationships between the relative intensity and the chosen elements. The total LREE's do not correlate with the relative intensity. As the intensity increased, the samples began to decrease, increased, and then decreased again. The graph of the wt% PbO followed this trend. This can be concluded to be a negative correlation. In looking at the end-members, all three showed correlations. The Ca, when plotted against the relative intensity, showed a decrease in percentage, i.e. concentration, as the intensity rose. This trend continued with the elemental wt% FeO graphs. The opposite of this occurred with the K. As the concentration of K in the sample grew, so did the relative intensity. The Na also did not show a consistent correlation, as the intensity increased, the concentration increased, then subsequently dropped off.

4.5 X-Ray Mapping and Chemical Analysis

Qualitative x-ray mapping was completed using the JEOL Subperprobe. This was done on five of the seven polished sections created from the samples. One of these samples, however,

was determined not to be a feldspar group mineral and the data for that sample was not used. Quantitative analysis was also completed on 5 polished sections. These samples were 303, 414, Ten Mile Bay, VIII-7-4 and VIII-11-1.

4.5.1 X-Ray Maps

Using the petrographic descriptions and the UV light pictures, key areas were marked for further analysis. These areas were chosen because of their increased fluorescing intensity. These areas included features such as zoning, exsolutions and inclusions. The three best examples of these are: (1) plagioclase zonation within diorite (sample 414) that showed variations in fluorescing intensities, (2) variations in fluorescence within perthitic exsolutions in orthoclase (sample 303), and (3) intensely fluorescing micro-inclusions within a dimly fluorescing labradorite (sample TMB). Below are the three x-ray maps for the above features. All of the element maps can be found in Appendix C.

4.4.1.1 Sample 414

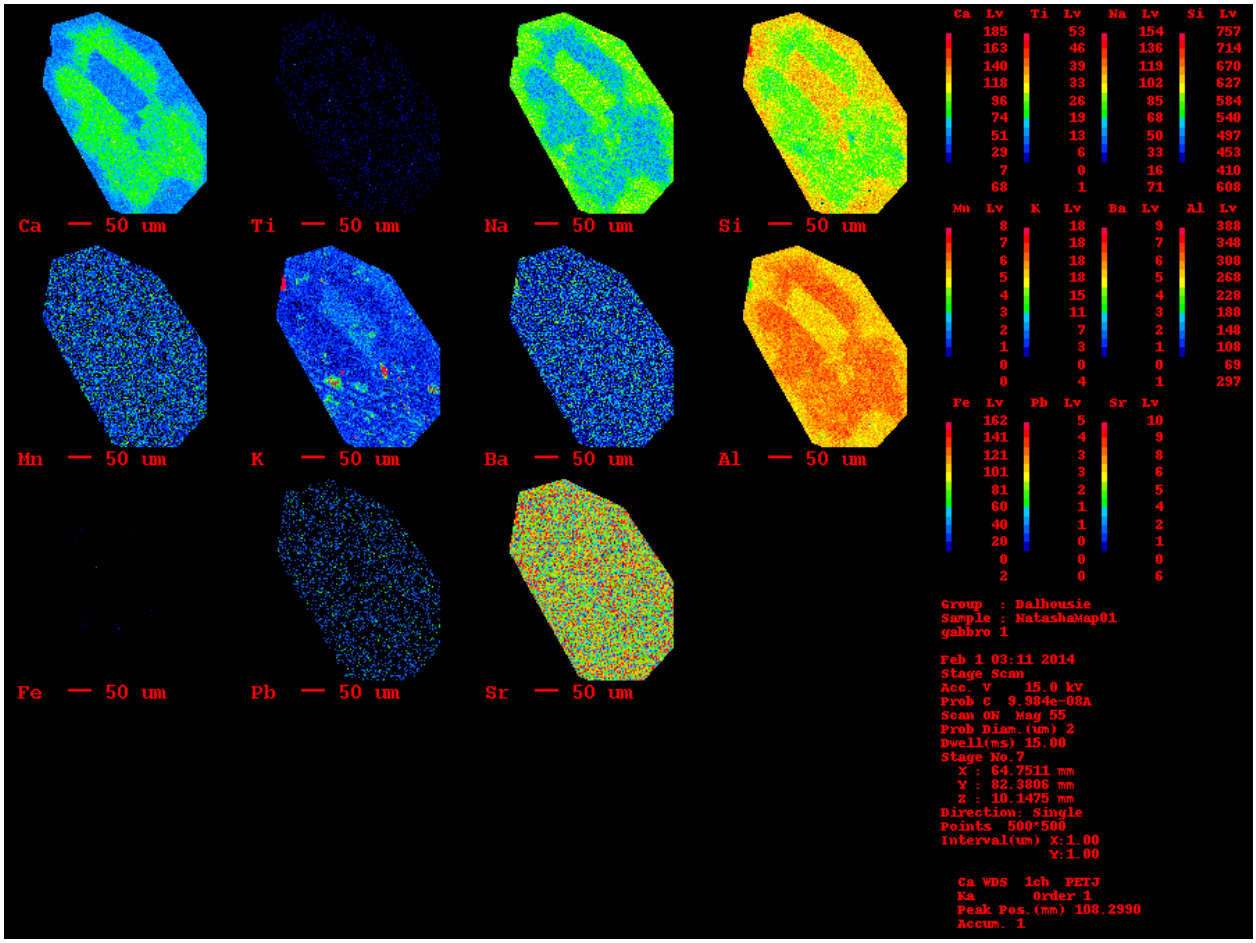

Figure 19: A 400um x 400 um x-ray map of a zoned andesine. Though the scales for each element are different, the cold colors represent low percentages while the warm represent high. The zoned andesine fluctuates in Ca, Na, Si, and Al.

The x-ray map above (Fig. 19) is of a zoned andesine crystal within the diorite. Looking at this crystal under UV light, the intensity of the fluorescence varies with the compositional changes. This phenomenon made this crystal an ideal candidate for x-ray analysis. This analysis showed variations in Ca, Na, Si, and Al. This variation corresponds with the variation in fluorescence. This means, the more Na rich areas fluoresced at a higher intensity then the Ca rich areas. The zonation in the fluorescence can be seen in Fig. 7.

4.4.1.2 Sample 303

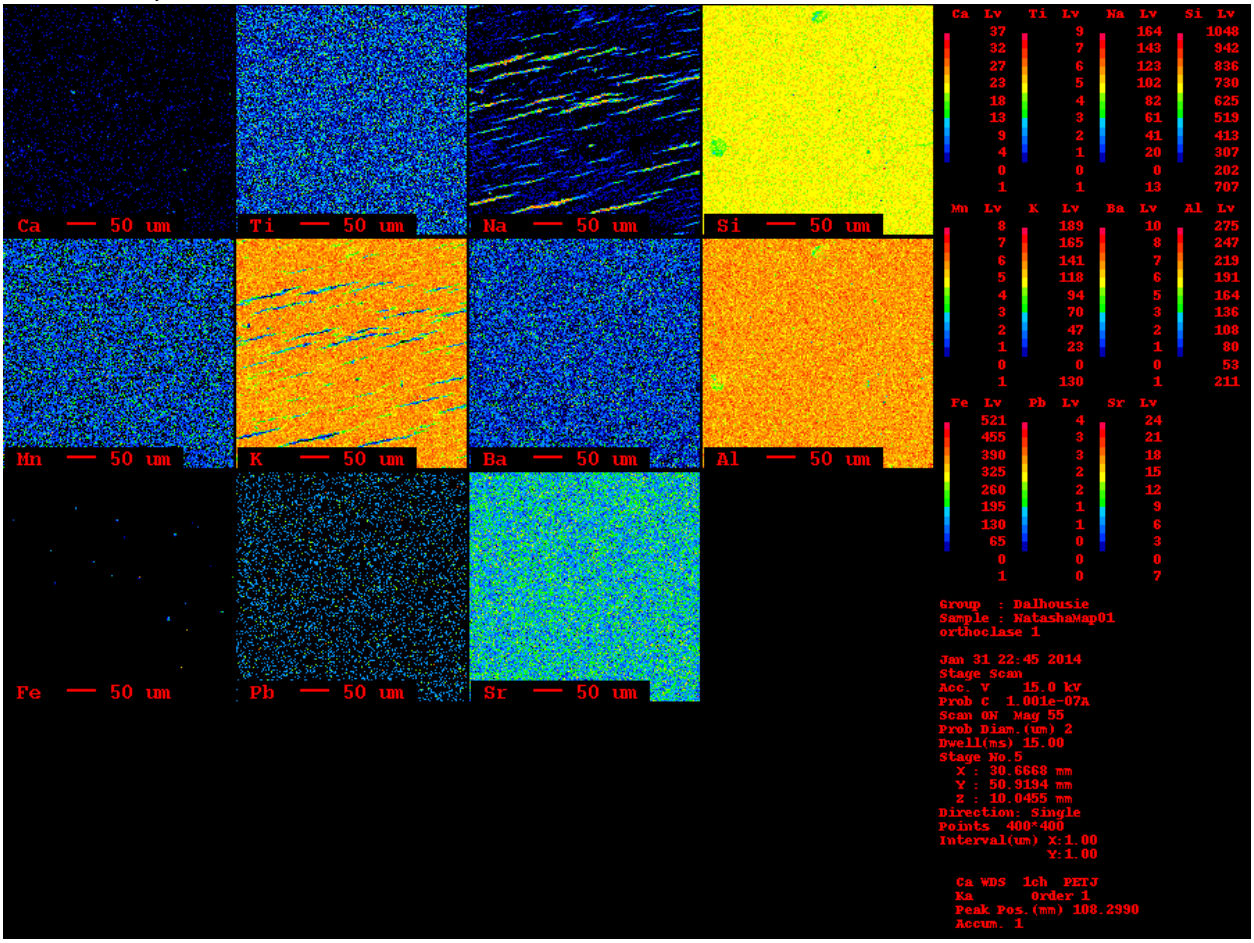

Figure 20: A 400um x 400um x-ray map of an orthoclase with perthitic exsolutions. With cold colors representing low percentages and warm representing high, this map shows a variation in K and Na thoughout the host minerals and exsolutions.

The orthoclase showed great promise with the fluorescence. The body of the mineral fluoresced a bright pink, whereas its perthitic exsolution lamellae fluoresced very dimly or not at all (Fig. 6). For x-ray analysis, K and Na were the main targets (Fig. 20). The body of the mineral was enriched in K and showed very low levels of Na. The exsolutions, however, were depleted in K and showed much higher levels of Na. The patterns on the map followed the fluorescing patterns of the mineral.

4.4.1.3 Sample TMB

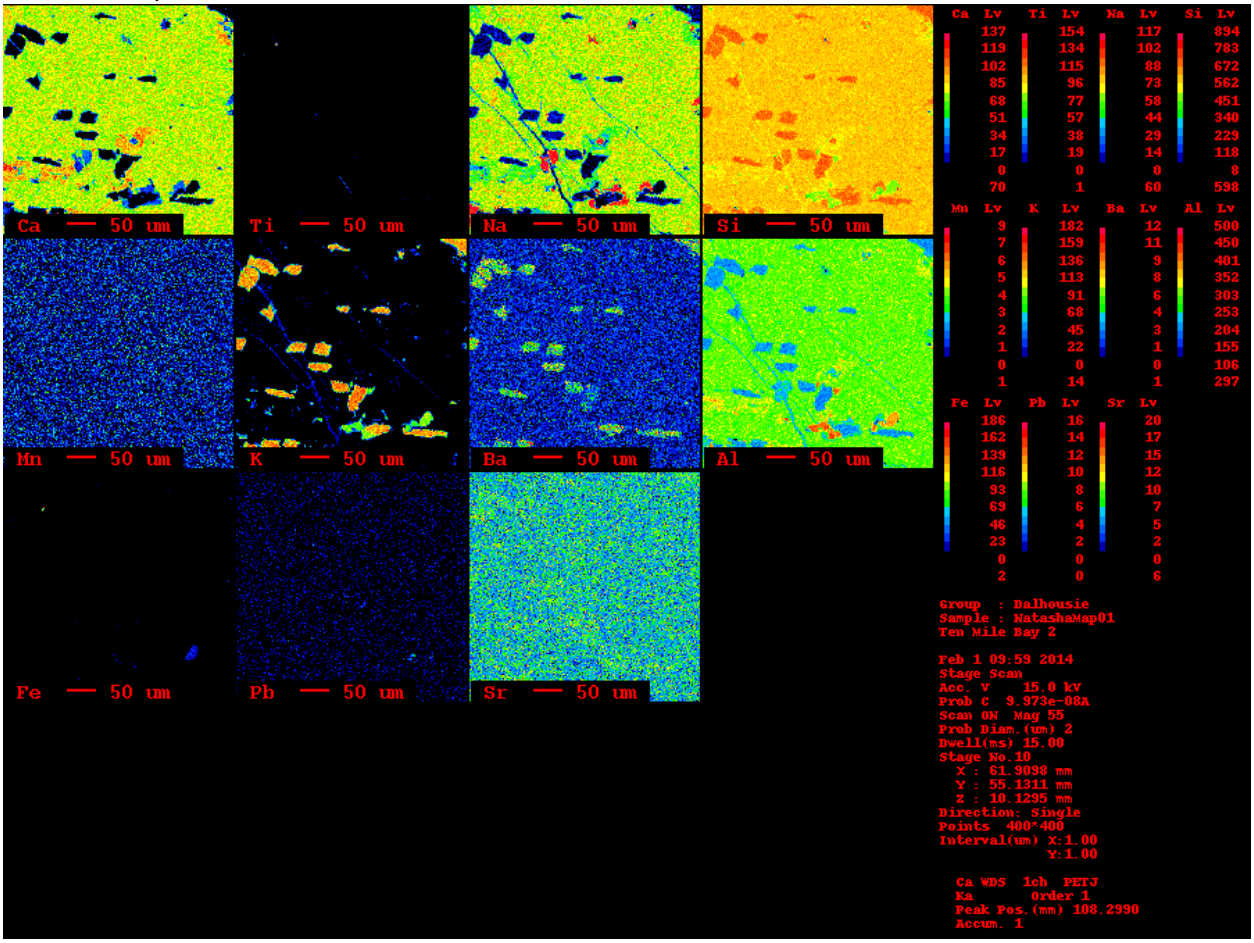

Figure 21: A 400um x 400um x-ray map of a labradorite with micro-inclusions. With cold colors representing low percentages and warm representing high, this sample shows variations in Ca, Na, K, Ba, and Al thoughout the host mineral and the micro-exsolutions.

Sample TMB was a very low intensity fluorescing labradorite. This labradorite had brightly fluorescing “flames” or micro-inclusions throughout (Fig. 9). Figure 15 shows a 400 um area of these micro-inclusions, which show a significantly different feldspar composition. The body of the mineral was enriched in Ca, Na, and Al. The micro-inclusions, in contrast, contain lower Ca, Na, Al and higher amounts of K and Ba.

4.5.2 Chemical Analysis

Chemical analysis was completed using an electron microprobe. Sample points were picked using the data collected from the fluorescent micrograph images and the x-ray maps. The microprobe data were collected for five of the thin sections: microcline, orthoclase, bytownite, diorite, and labradorite. Points were taken in the body of the mineral, the edge of the exsolution or the inclusion, and the inside of the exsolution or the inclusion. Below are the end-member percentages of all points analyzed in tri-plot form. The probe data were analyzed using a normalization equation that evaluated oxide weight percent into percent anorthite, albite, and orthoclase. This was then transferred into the tri-plot program so that each point could be plotted and its true composition shown. The full set of microprobe analyses is in Appendix D.

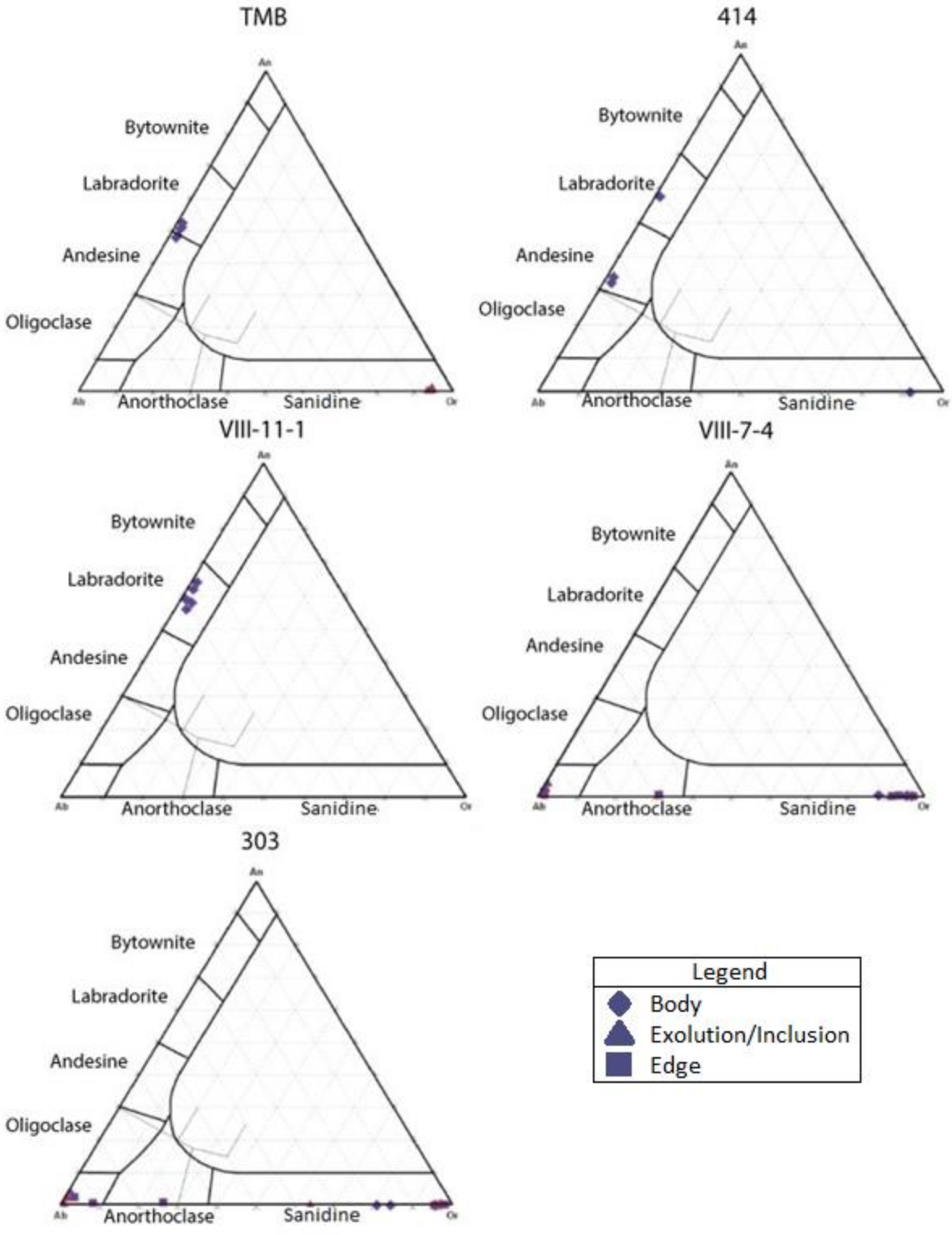

Figure 22: Five tri-plots of the 5 analyzed samples. This shows the percent An, Ab, and Or calculated from the probe data.

4.5 Crystal Structure Modeling

Crystal models of pure forms of orthoclase, microcline, albite and anorthite were created using *CrystalMaker* and based on the compositions of the samples as analyzed via microprobe. Thus, these crystal models do not take into consideration any changes in crystal structure caused by substitutions in the chemical composition. However, we can assume that major element substitutions will produce mixtures between these end-members and that trace-element substitutions will have little measureable effect on the crystal structure. The crystal models were then used to produce synthetic x-ray diffraction data using *CrystalDiffract*. The objective of this experiment was to show the difference in the unit cell parameters between the crystal structures for each of the main end-members. This data could then be compared with the fluorescence data, to see if there is a correlation between the structure of the mineral and the intensity of the fluorescence. The models and diffraction data are shown in Figure 23, 24, 25, and 26.

The link between the crystal structure and fluorescence can be seen by looking at the unit cell parameters. Firstly, the unit cell parameter distances (a, b and c) all decrease from orthoclase to anorthite. Taking the largest unit cell parameter (b) the size changes from 12.963 Å, to 12.96 Å in the K-feldspars (orthoclase and microcline), to 12.87 Å for albite and 12.785 Å for anorthite. The wavelength for shortwave UV sources is clearly much larger than the distances between the atoms in these minerals. We can therefore consider the interaction of UV photons as a volume interaction and excitation. For the smaller unit cell parameters (a and c) the variations are similar in that they decrease from orthoclase (a = 8.563 Å, c = 7.299 Å) to anorthite (a = 8.177 Å, b = 7.158 Å). These unit cell parameter variations represent maximum

variations in volume between orthoclase and anorthite unit cells of 810.205 Å^3 and 748.318 Å^3 respectively. This suggests a unit cell volume difference between pure orthoclase and anorthite of 7.64%. This finding is not surprising, given the difference in specific gravity between these end-members of 2.55 g/cm^3 and 2.76 g/cm^3 (Ness, 2012). In terms of UV photon interaction, this means that there could be as much as 7.64% more photon-atom interactions in the same volume of anorthite versus orthoclase.

The other unit cell parameters, namely the angles between the crystallographic axis, are also different. Orthoclase is monoclinic with the β angle at 116.6^o (Fig. 23). The β angles for all the feldspars are close to this value. Microcline is marginally triclinic with the α and ɤ angles only slightly off set from 90^o (Fig. 24). Plagioclase feldspars are triclinic with the α and ɤ angles crystallographic angles increasingly offset from 90^o (Figs. 25 and 26). Again, In terms of UV photon interaction these parameters mean that, for the plagioclase feldspars, there would be a much greater chance of photon-atom interaction as there are no right angles in any of the crystal orientations. Also, as described above, the distances between the atoms are smaller.

The consequences for the observations in terms of the actual observed fluorescence and there measure major and trace-element contents in the natural samples are discussed in the next section.

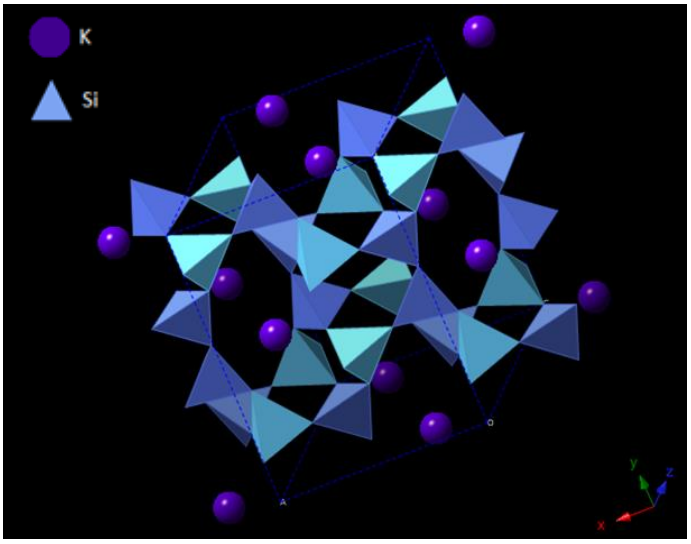

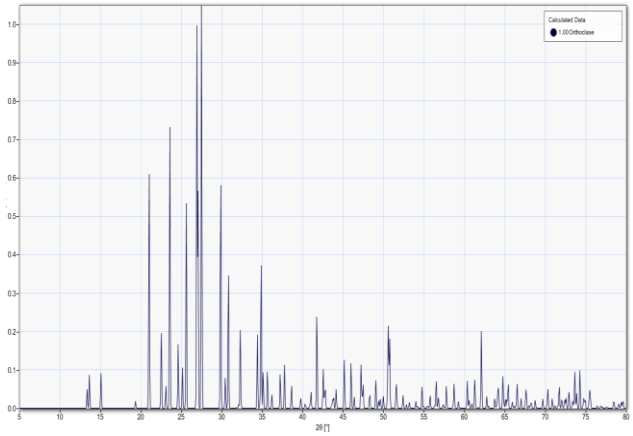

a= 8.563 Å b= 12.963 Å c= 7.299 Å
β= 116.60°

Figure 23: An orthoclase crystal, diffraction spectrum and corresponding unit cell parameters. The structure was created using CrystalMaker and the diffraction spectrum by CrystalDiffract.

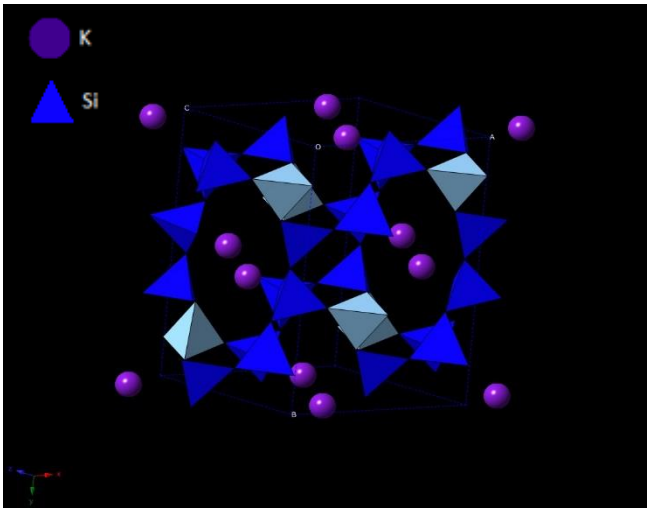

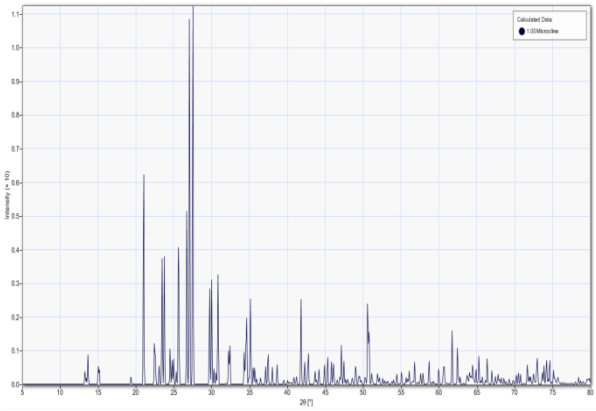

a= 8.578 Å b= 12.960 Å c= 7.211 Å
α= 90.65° β= 115.96° γ= 87.65°

Figure 24: A microcline crystal, diffraction spectum and corresponding unit cell parameters. The structure was created using CrystalMaker and the diffraction spectrum by CrystalDiffract.

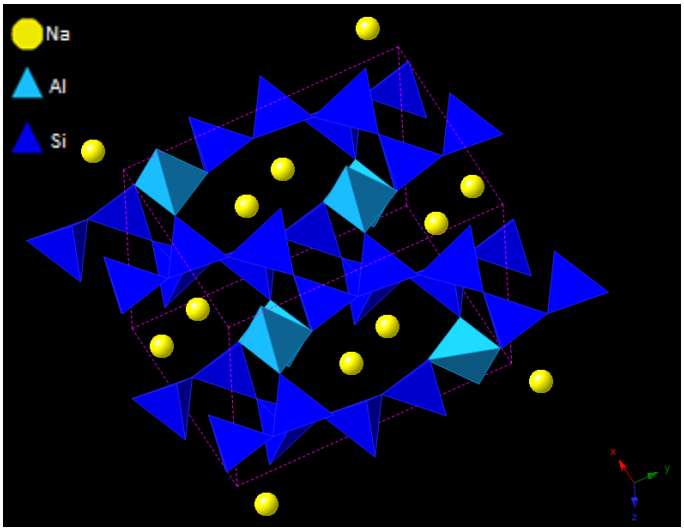

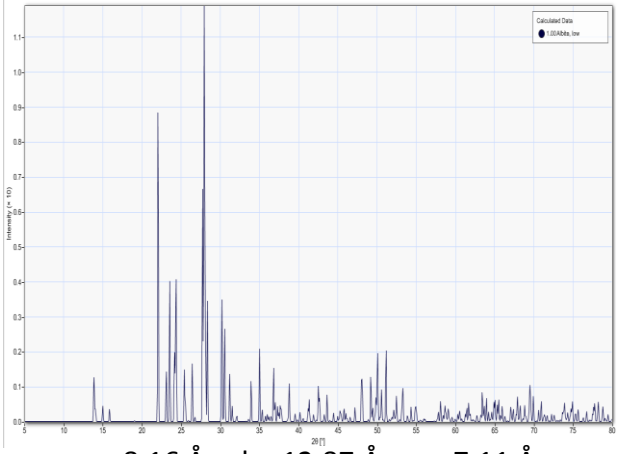

a= 8.16 Å b= 12.87 Å c= 7.11 Å
α= 93.45° β= 116.4° γ= 90.28°

Figure 25: An albite crystal, diffraction spectrum and corresponding unit cell parameters. The structure was created using CrystalMaker and the diffraction spectrum by CrystalDiffract.

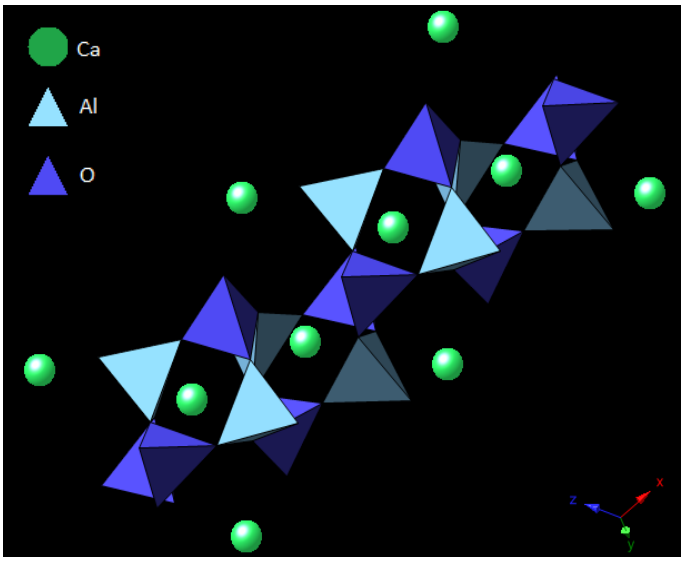

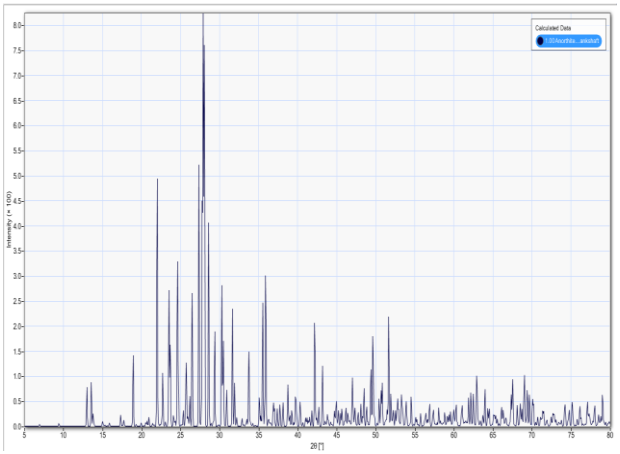

a= 8.177 Å b= 12.785 Å c= 7.158 Å
α= 94.26° β= 116.60° γ= 87.71°

Figure 26: An anorthite crystal, diffraction spectrum and corresponding unit cell parameters. The structure was created using CrystalMaker and the diffraction spectrum by CrystalDiffract.

5.0 DISCUSSION AND CONCLUSIONS

5.1 Discussion

The data analyzed within this thesis yielded some interesting results. Firstly, looking at the large unmounted samples, it was evident that all of them fluoresced to some extent. Furthermore, these samples all seemed to fluoresce in different shades of red/pink meaning they are most likely fluorescing within the red wavelength, i.e. between 640-720nm. These initial observations indicate that the potassium feldspars fluoresced with a much greater intensity than did the plagioclase feldspars. The only exception to this would be the Ten Mile Bay labradorite. In hand-sample, it fluoresced with an intense pink color, much like that of the orthoclase. This can be explained as follows. This unmounted sample was the only polished large sample, meaning the UV light will reflect much more brightly off the surface, giving it the more intense apparent fluorescence. Furthermore, in looking at the micrographs and the x-ray maps, it is evident that there is an abundance of K-feldspar micro-inclusions throughout this sample. These were also seen to fluoresce much more intensely than the host plagioclase. In short, the bulk fluorescence observed might actually be attributed to these inclusions, and as the K-feldspar micro-inclusions are distributed throughout the sample, this account for the apparent overall fluorescence.

The response to UV light observed using the thin sections produced several interesting observations. Three samples stood out in this regard, the orthoclase (sample 303), the Ten Mile Bay labradorite (sample TMB) and the andesine crystals within the diorite (sample 414). The large specimen sample of the orthoclase fluoresced with a very intense pink color. In thin section, the body of the mineral was indeed seen to be fluorescing in this same overall color. In

contrast, the perthite exsolutions did not seem to fluoresce as intensely, if at all. On the basis of the x-ray maps and microprobe data, the perthite exsolutions were much lower in K and were, not surprisingly, composed of albite. This leads to the initial hypothesis that it is an activator located within potassium feldspar minerals that is causing the fluorescence.

As described above, the Ten Mile Bay labradorite hand sample also showed intense pink fluorescence. However, from the thin section, it was evident that the object fluorescing was micro-inclusions within the mineral. Though the host mineral had some, rather low-intensity fluorescence, these micro-inclusions showed intense pink fluorescence and were highly potassic. This supports the hypothesis that it is indeed an activator(s) element within the potassium feldspar structure that is causing the fluorescence. It is therefore likely that an element which is preferentially substituting into the crystal structure for K, and which will not fit easily into the structure of plagioclase feldspar, that produces the observed fluorescence. For example, the K-feldspar micro-inclusions also have increased levels of barium which could be aiding in the fluorescence.

The plagioclase within the diorite also showed interesting results. The zoned plagioclase crystals showed significant variation in the intensity of the fluorescence. When analyzed, the crystals showed variation in composition from labradorite to andesine and had overgrowths of sanidine/orthoclase. These overgrowths fluoresced with the most intensity. In another sample, the crystal fluctuated between more Ca and more Na rich, with the Na-rich samples showing a more intense fluorescence.

From these data, it is evident once again that the potassium-rich end-members had the most intense fluorescence, whereas the calcium end-members seemed to have decreased intensity with increased percentage of Ca. The sodium end-member, being the composition link between the orthoclase and Ca-rich feldspar, showed moderate fluorescence throughout. These results lend further support the hypothesis that it is the K-feldspars that contain an activating element in the crystal structure which is responsible for, and correlates with, the highest intensity of fluorescence in feldspar minerals. However, the major flaw with this hypothesis is that the total LREE and Fe contents are ***negatively*** correlated with fluorescence. In other words the K-feldspars all have significantly less of these potential activator elements that the plagioclase feldspars examined in this study. It is therefore likely that a secondary effect or parameter must be contributing to the clear difference in fluorescence.

High resolution studies (i.e. EMP and LA-ICP-MS) showing the distribution of Fe in feldspars have concluded that in orthoclase Fe is typically present at low concentration (<300 ppm) and is in fact present mainly as nano-inclusions of oxide phases which range in composition from Fe-Ti rich to Fe-rich (Parsons et al. 2008). Conversely, Fe contents in plagioclase are significantly higher than in orthoclase (>700-1200 ppm) and Fe is clearly incorporated into the crystal structure rather than nano-inclusions (Lee et al. 2007). The Fe contents have also been shown to be redistributed between Or-rich and Ab-rich components of crystals which have undergone sub-solidus exsolution (Parsons et al. 2009). Thus, we can conclude that the Fe contents in plagioclase feldspar crystals are both higher that for K-rich crystals and that Fe is present within the plagioclase mineral structure rather than as sub-microscopic inclusions. This, along with the clear inverse correlation between UV intensity and

Fe-contents, suggests that Fe may be acting as a quenching element which reduces the intensity of the UV florescence in plagioclase. In contracts, Fe contents have no damping effect on the florescence in K-feldspars as the Fe atoms are present at much lower concentrations, and indeed not all Fe atoms are even contained within the crystal structure. Therefore the effect of Fe-quenching within K-feldspars is greatly reduced compared to plagioclase crystals. Further work would need to be done however to determine if this Fe was ferric or ferrous, as it is the ferrous Fe that causes the quenching.

The biggest differences in the crystal structures of these minerals are that the orthoclase has a monoclinic crystal symmetry and larger unit cell parameters, whereas anorthite to albite have a triclinic structure and are closer packed, thus have smaller unit cell parameters. This change in symmetry might also affect the fluorescence. In the case of the monoclinic structure the wider spacing between the atoms and the right angled crystal axes might allow greater channeling of photons both into and through the crystal lattice. This would in turn increase the amount of volume interactions between the UV photons and the activator elements within the K-feldspar crystals. A similar channeling effect has been noted for electrons in zircon crystals (Nasdala et al., 2006). In the case of plagioclase, the crystal structures all have smaller spacing between the atoms and an absence of right angled crystal axes. This would result in a greater interaction between UV photons and atoms but would also result in greater scattering and absorption of the UV light much closer to the samples surface than for K-feldspars. This, in turn, might result in much lower volumes of UV stimulated emission and this may explain the apparent differences in fluorescence and the negative correlation with apparent trace-element activators. Finally, there may be other activators or enhancer elements

which were not detected by the electron microprobe. A combination of activators and enhancers, which are concentrated together in the K-feldspars, may also explain the higher intensity fluorescence. However, this could only be tested by measuring the trace-elements present with more sensitive analytical methods, such as ion microprobe or laser ablation ICP-MS, and by looking at UV spectroscopy to determine which elements are indeed responsible for the fluorescence.

5.2 Conclusions

The conclusions are:

- UV fluorescence is positively correlated with the K-feldspar (orthoclase) end-member.
- There is an inverse negative correlation between the concentration of common activator elements (such as LREE and Fe) and the intensity of fluorescence. In short, plagioclase has much higher LREE and Fe contents but shows significantly less intense fluorescence.
- Plagioclase feldspars have a higher concentration of Fe within their structure then K-feldspars. Since Fe is a quencher, this could be a cause of plagioclase feldspars less intense fluorescence.
- K-feldspars, are clearly much more fluorescent than plagioclase crystals and it is likely that it is a combination of the crystal structure, activator and the lack of Fe in the crystal structure that results in the more intense fluorescence.

- The significant structural changes from orthoclase (monoclinic) to anorthite (triclinic) along with the very different unit cell parameter's may also produce intrinsic difference in the UV responses, or enhance the effects of LREE activation and/or Fe quenching

5.3 Future Work

UV spectroscopy will be required to further understand the link between variation in major or trace elements and the fluorescent spectra. Quantitative microprobe analysis using a more sensitive method will also be required to identify these variations. Furthermore, X-Ray diffraction should be done on the samples to identify the full crystal-chemical make-up of the minerals. Finally, a determination of Fe content, Fe^{2+} or Fe^{3+}, would have to be completed to identify whether or not it is indeed the ferrous Fe causing the fluorescence quenching in plagioclase feldspars.

6.0 REFERENCES

Barbieri, B. 2012. A Short History of Fluorescence. The Fluorescence Foundation. Pp 3-14.

Burgess, A., Vigneron, S., Brioudes, E., Labbé, J-C., Lorca, T., and Castro A. 2010. Loss of human Greatwall results in G2 arrest and multiple mitotic defects due to deregulation of the cyclin B-Cdc2/PP2A balance. *Proc Natl Acad Sci USA* 107: 12564–12569

Davidson, Michael and the Flordia State University. 2012. Basic Concepts in Fluorescence. Florida State University. http://micro.magnet.fsu.edu/primer/techniques/fluorescence/fluorescenceintro.html Accessed September 14th, 2013.

Elkins, L. T., & Grove, T. L. 1990. Ternary feldspar experiments and thermodynamic models. American Mineralogist, 75, 544-559.

Goldstein, J., Newbury, D., Joy, D., Lyman, C., Echlin, P., Lifshin, E., Saywer, L., and Michael, J. 2003. Scanning electron mircoscopy and x-ray analysis (3rd ed.). New York City: Springer Science.

Fluorescent Mineral Society. 2013. Fluorescent Minerals. http://uvminerals.org/fms/about-fluorescent-mineral-society. Accessed September 14th, 2013.

Gaft, M., Naqli, L., Panczer, G, Waychunas., G and Porat, N. 2008. The nature of unusual luminescence in natural calcite CaCO3. American Mineralogist, 73(1): 158-167.

Hamblen, James O. Fluorescent Minerals. Georgia Tech. http://users.ece.gatech.edu/~hamblen/uvminerals/ Accessed September 14, 2013.

Krbetschek, M. R., Götze, J., Dietrich, A., and Trautmann, T. 1997. Spectral information from minerals relevant for luminescence dating. Radiation Measurements, 27: 695–748.

Lee, M. R., Parsons, I., Edwards, P. R., and Martin, R. W. 2007. Identification of cathodoluminescence activators in zoned alkali feldspars by hyperspectral imaging and electron-microprobe analysis. American Mineralogist, 92: 243-253.

Modreski, Peter J. 1987. Ultraviolet Fluorescence of Minerals; examples from New Mexico. New Mexico Geology – Science and Service. 9(2): 25-42.

National Audubon Society. 1979. Field Guide to Rocks and Minerals; North American Ed. National Audubon Society Field Guides.

Nasdala, L., Krontz, A., Hanchar, J.M., Tichomirowa, M., Davis, D.W., Hofmeister, W. 2006. Effects of natural radiation damage on back-scattered electron images of single crystals of minerals. American Mineralogist, 91: 1739–1746.

Parsons, I., Steele, D. A., Lee, M. R., and Magee, C. W. 2008. Titanium as a cathodoluminescence activator in alkali feldspars. American Mineralogist, 93: 875-879.

Parsons, I., Magee, C. W., Allen, C. M., Shelley, J. M. G., and Lee, M. R. 2009. Mutual replacement reactions oin alkali feldspars II: trace element partitioning and geothermometry. Contrib Mineral Pertol, 157: 663-687.

Przibram, K. 1956. Irradiation Colours and Luminescence. Pergamon Press.

Schneider, Stuart. 2004. Collecting Fluorescent Minerals. Schiffer Publishing, Ltd. Pp. 8-10.

Smith, J. V., and Brown, W. L. 1974. Feldspar Minerals: 1 Crystal Structures, Physical, Chemical, And Microtextural Properties (2nd ed). Germany: Springer-Verlag.

Winter, J. D. 2010. Principles of igneous and metamorphic petrology (2nd ed.). Upper Saddle River, NJ: Prentice Hall.

APPENDIX A

Sample Number	Composition of Feldspar	Fluorescent	Intensity	Cause of Fluorescence	Features/ Textures
303	Orthoclase	yes	high	bulk of mineral	Exsolutions/ Perthite
414	Andesine	yes	fair	Na rich plagioclase	Twinning/ Zonation
446	Andesine	yes	low	Na righ plagioclase	Twinning
TMB	Labradorite	yes	high	micro-inclusions	Micro-Inclusions
VIII-11-1	Labradorite	yes	low	labradorite	Twinning
VIII-7-4	Microcline	yes	high	bulk of mineral	Twinning/ Perthite
VIII-9-2	Oligoclase	yes	fair	Na rich plagioclase	Twinning

APPENDIX B

	TMB Body 1	TMB Body 2	TMB Body 3	TMB Inc 1	TMB Inc 2	TMB Inc 3	Orthoclase Body 1	Orthoclase Body 2	Orthoclase Body 3	Orthoclase Ex 1
La2O3	0	0	0.03	0	0.005	0	0	0.013	0	0.004
Y2O3	0	0	0	0	0	0	0	0	0	0
Pr2O3	0.022	0.03	0.004	0	0	0	0.023	0	0.019	0
Ce2O3	0.004	0.014	0.012	0.016	0.049	0.028	0	0	0.014	0
Nd2O3	0	0.043	0.016	0	0	0	0.035	0	0	0
Dy2O3	0	0	0.017	0	0	0.028	0.065	0.037	0	0
Eu2O3	0	0.043	0	0.014	0.007	0.004	0.032	0	0.047	0
Sm2O3	0	0	0	0	0	0	0	0	0.009	0
Gd2O3	0.006	0	0.062	0	0	0	0.009	0.046	0.001	0.005
CaO	7.612	7.612	7.612	0.064	0.064	0.064	0.01	0.01	0.01	0.317
Na2O	4.131	4.131	4.131	0.421	0.421	0.421	0.752	0.752	0.752	8.362
K2O	0.291	0.291	0.291	12.42	12.42	12.42	12.355	12.355	12.355	0.095
TiO2	0	0	0	0	0	0	0	0	0	0
Al2O3	14.296	14.296	14.296	9.603	9.603	9.603	9.469	9.469	9.469	10.221
SiO2	22.839	22.839	22.839	26.111	26.111	26.111	26.778	26.778	26.778	28.262
FeO	0.156	0.156	0.156	0.036	0.036	0.036	0.026	0.026	0.026	0.009
MnO	0.002	0.002	0.002	0.004	0.004	0.004	0.004	0.004	0.004	0
BaO	0	0	0	1.237	1.237	1.237	0	0	0	0
SrO	0.033	0.033	0.033	0.033	0.033	0.033	0	0	0	0.018
PbO	0.034	0.034	0.034	0.034	0.034	0.034	0.043	0.043	0.043	0.027
O	50.606	50.606	50.606	50.609	50.609	50.609	50.563	50.563	50.563	52.688
Totals	100.032	100.13	100.141	100.602	100.633	100.632	100.164	100.096	100.09	100.008

Orthoclase Ex 2	Orthoclase Ex 3	Labradorite 1	Labradorite 2	Labradorite 3	Microcline 1	Microcline 2	Microcline 3	Diorite 1	Diorite 2	Diorite 3
0	0.017	0.023	0	0.003	0	0.004	0.037	0	0	0
0	0	0	0	0	0	0	0	0	0	0
0.019	0.031	0.009	0.052	0	0.031	0.004	0.038	0.004	0	0.029
0.03	0.065	0	0.008	0.008	0.027	0.01	0.006	0.02	0.03	0
0	0	0	0.008	0.072	0	0	0.062	0	0	0.034
0.05	0	0	0	0	0.047	0.035	0	0	0	0
0	0	0.019	0.043	0	0	0	0	0	0.013	0
0	0	0	0.056	0	0.002	0	0	0.032	0.001	0
0.009	0	0	0.054	0	0.067	0.026	0.01	0.07	0.008	0.012
0.317	0.317	9.143	9.143	9.143	0.019	0.019	0.019	6.312	6.312	6.312
8.362	8.362	3.31	3.31	3.31	0.451	0.451	0.451	4.963	4.963	4.963
0.095	0.095	0.273	0.273	0.273	12.992	12.992	12.992	0.233	0.233	0.233
0	0	0	0	0	0	0	0	0	0	0
10.221	10.221	15.397	15.397	15.397	9.438	9.438	9.438	13.709	13.709	13.709
28.262	28.262	21.735	21.735	21.735	26.62	26.62	26.62	23.93	23.93	23.93
0.009	0.009	0.175	0.175	0.175	0.018	0.018	0.018	0.096	0.096	0.096
0	0	0	0	0	0	0	0	0.002	0.002	0.002
0	0	0	0	0	0	0	0	0	0	0
0.018	0.018	0.027	0.027	0.027	0	0	0	0	0	0
0.027	0.027	0.046	0.046	0.046	0.006	0.006	0.006	0.03	0.03	0.03
52.688	52.688	49.894	49.894	49.894	50.456	50.456	50.456	50.725	50.725	50.725
100.107	100.112	100.051	100.221	100.083	100.174	100.079	100.153	100.126	100.052	100.075

APPENDIX C

Microprobe x-ray maps.

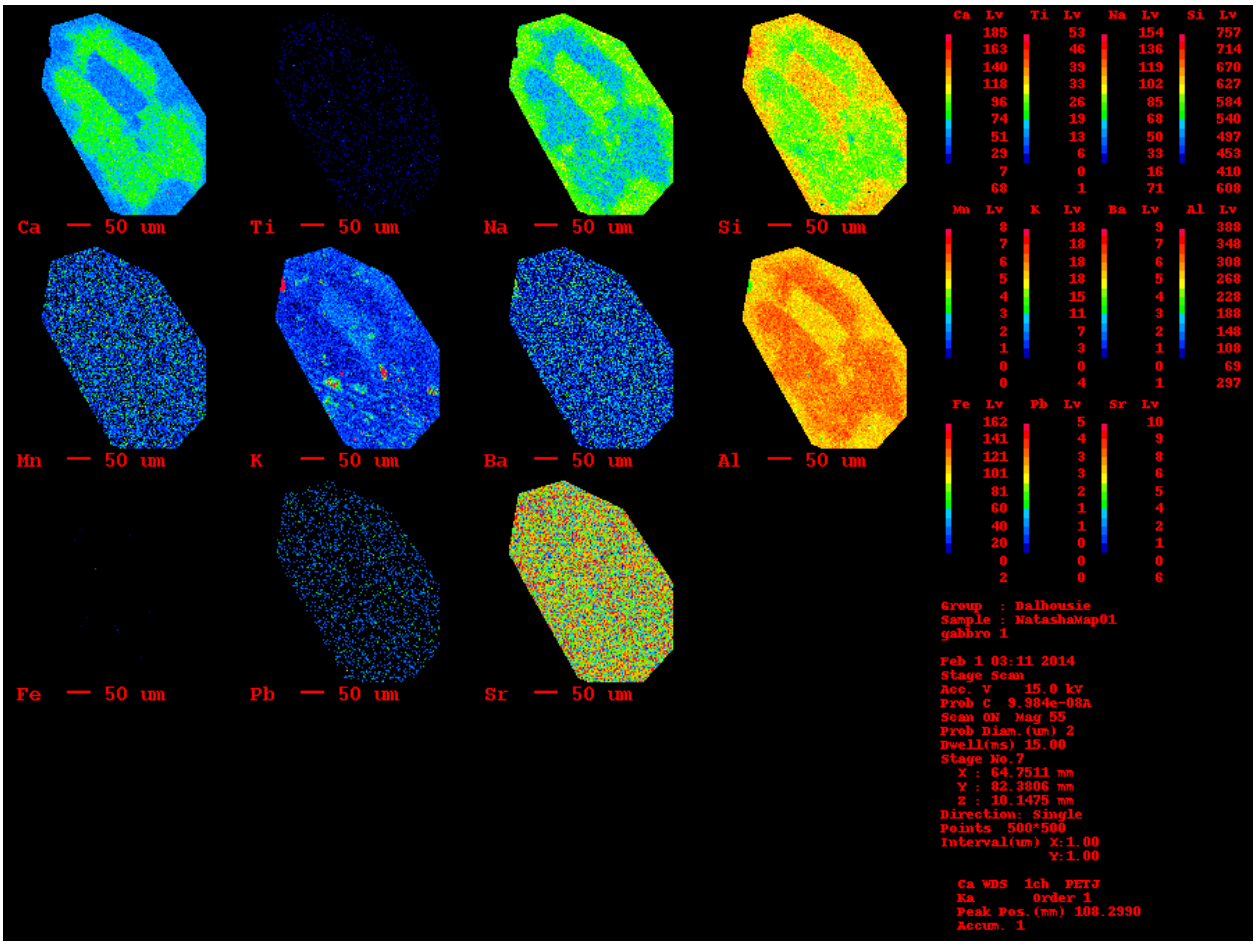

414 – Zoned Plagioclase in Diorite

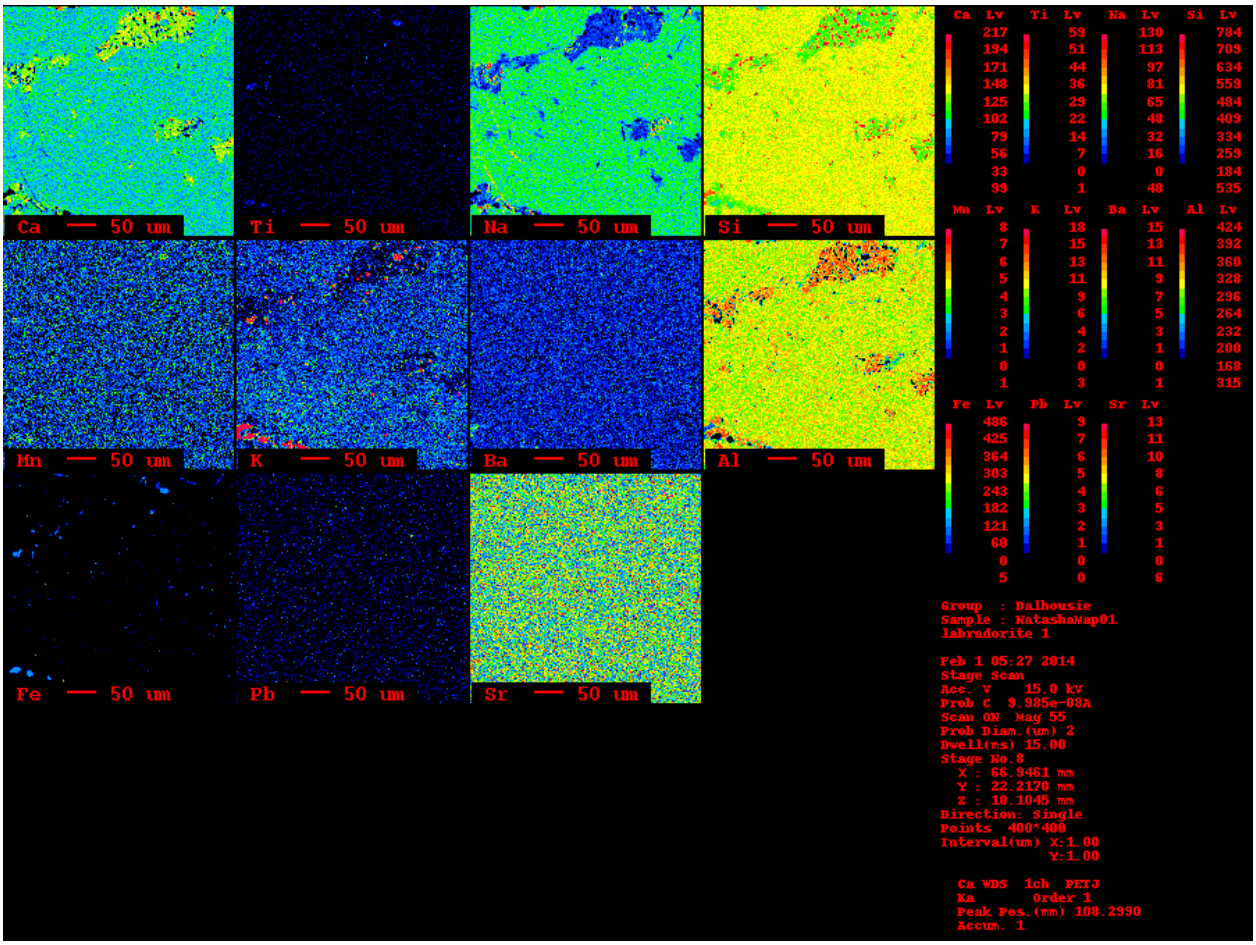

VIII-11-1 – Inclusions in Labradorite

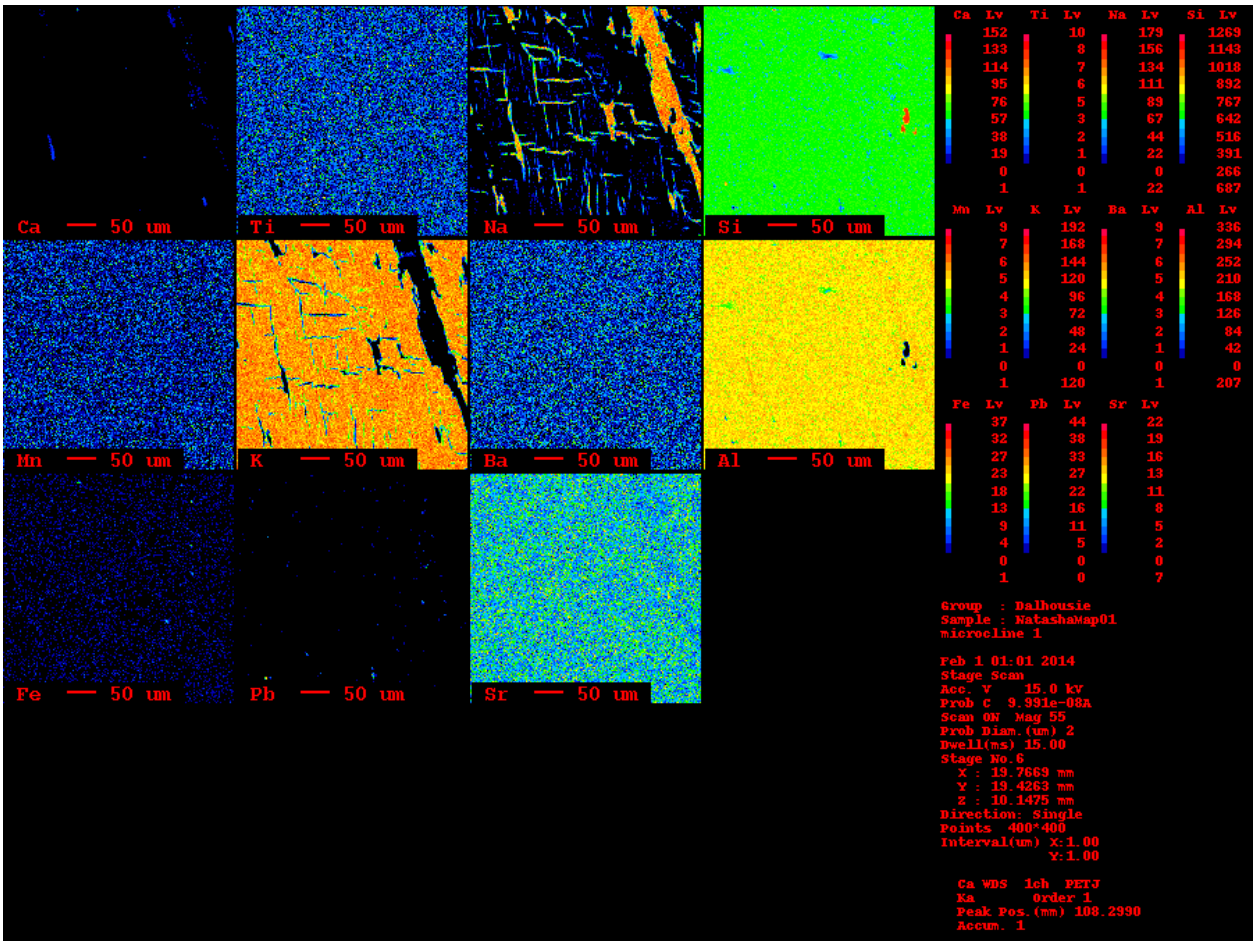

VIII-7-4 – Tartan Twinning in Microcline

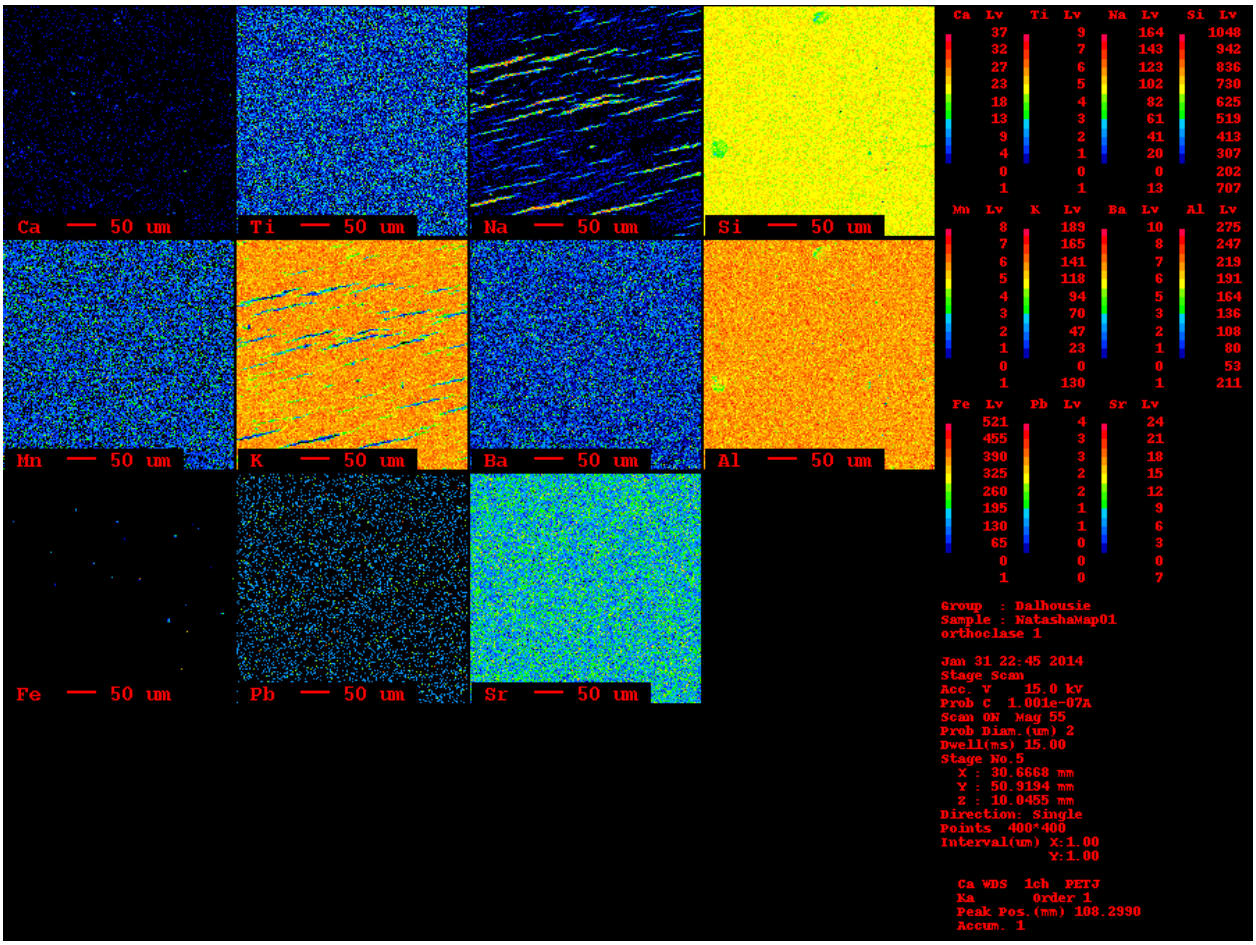

303-1 – Perthitic Texture in Orthoclase

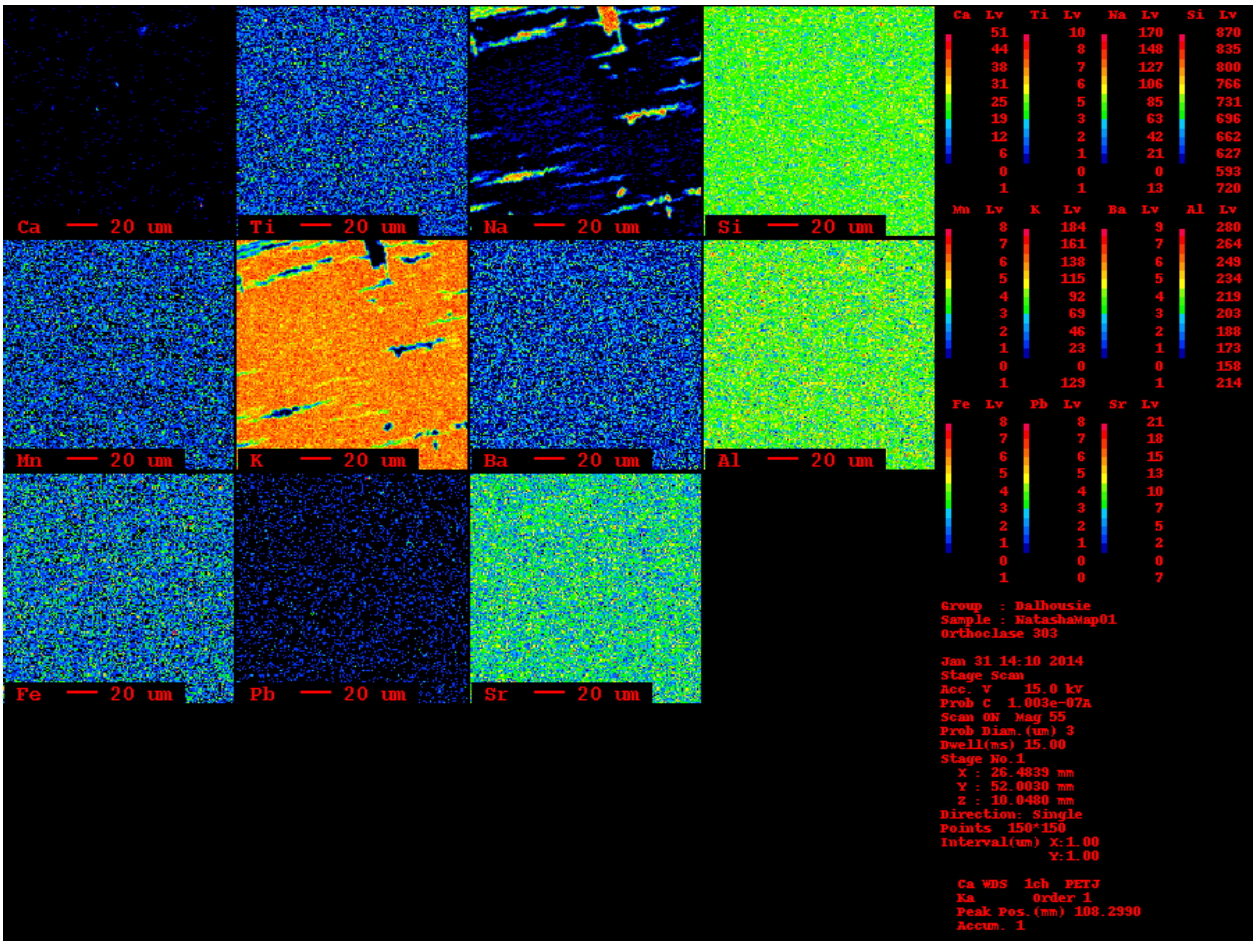

303-2 – Perthitic Exsolutions in Orthoclase

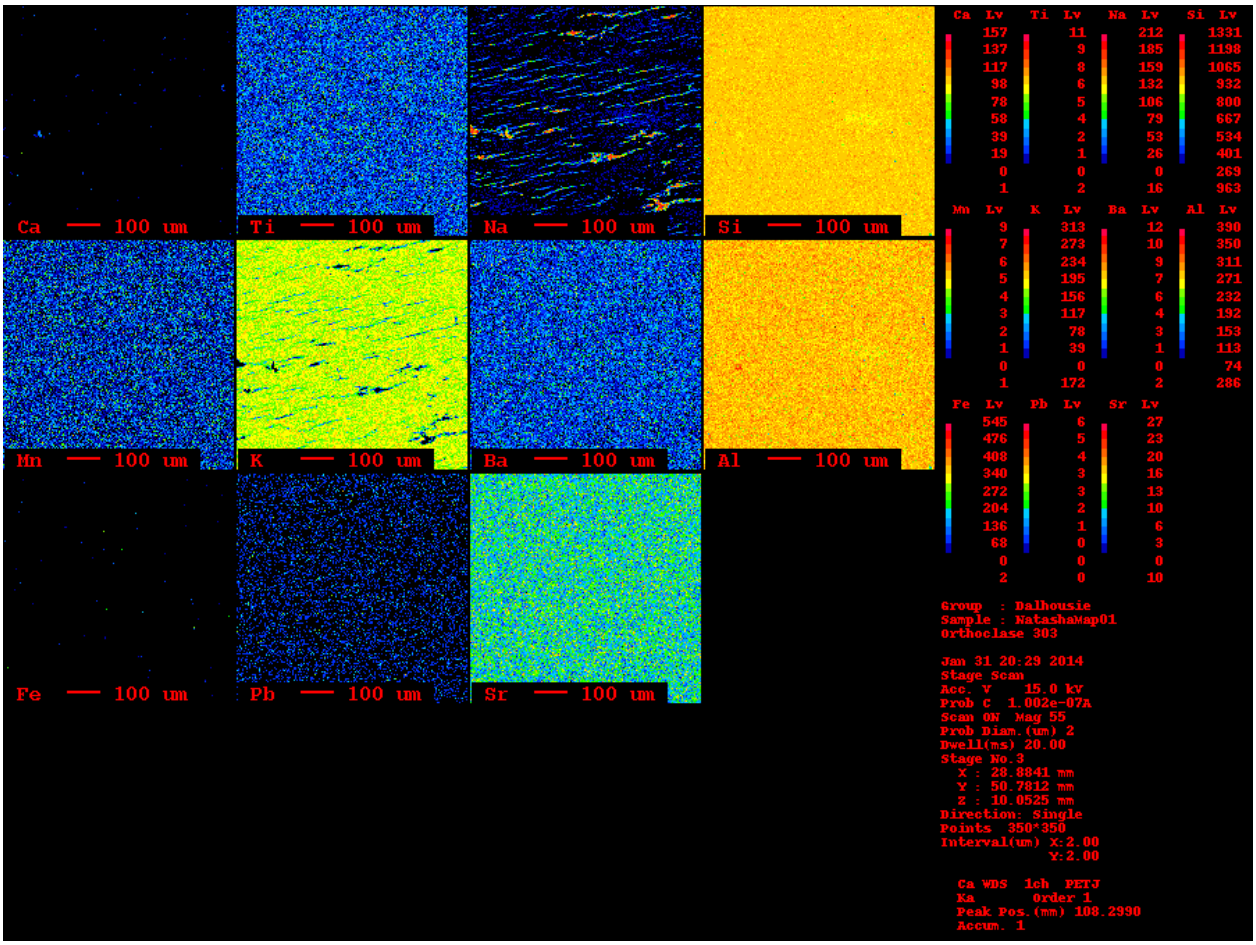

303-3 – Perthitic Texture in Orthoclase

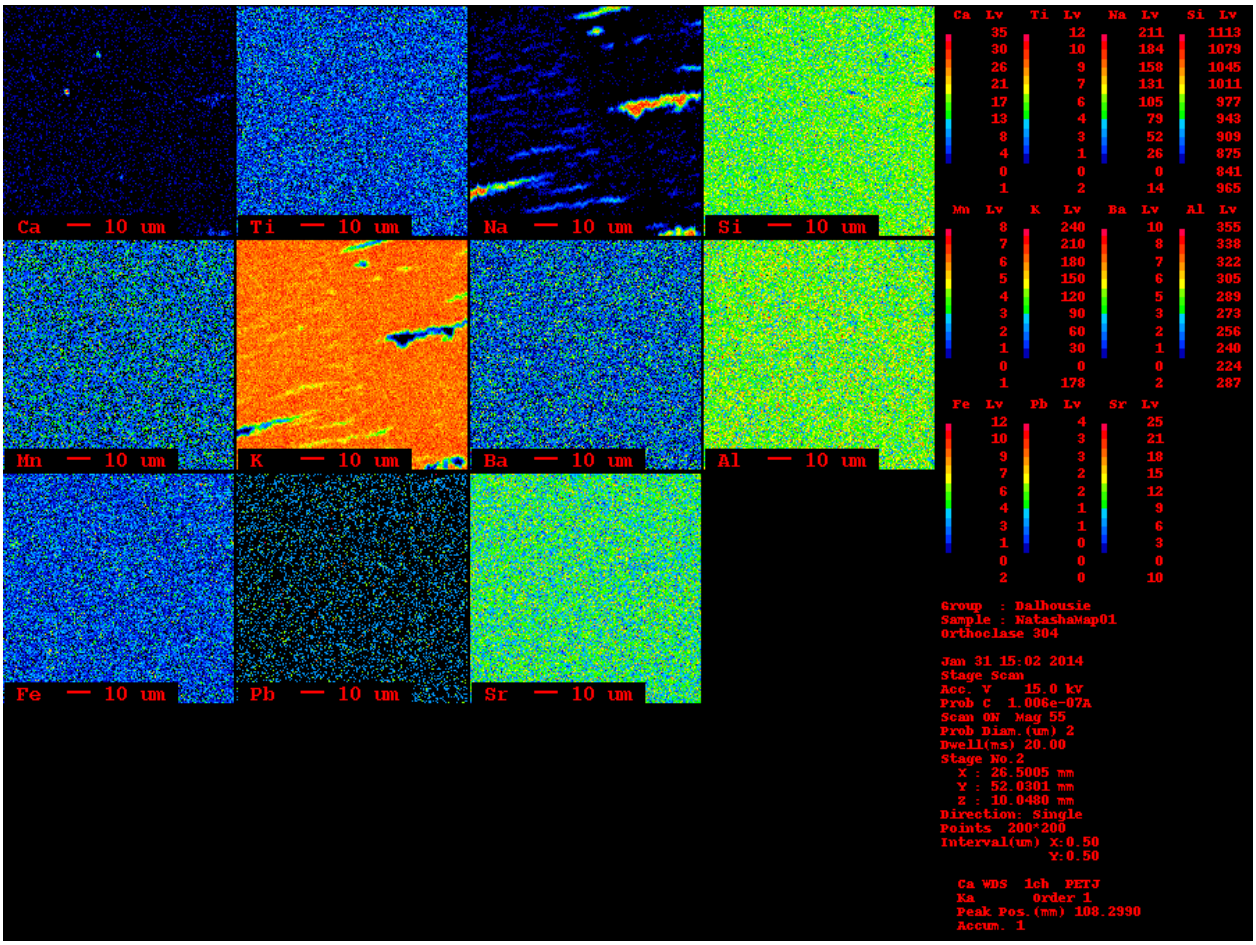

303-4 – Micro-exsolutions of Perthite in Orthoclase

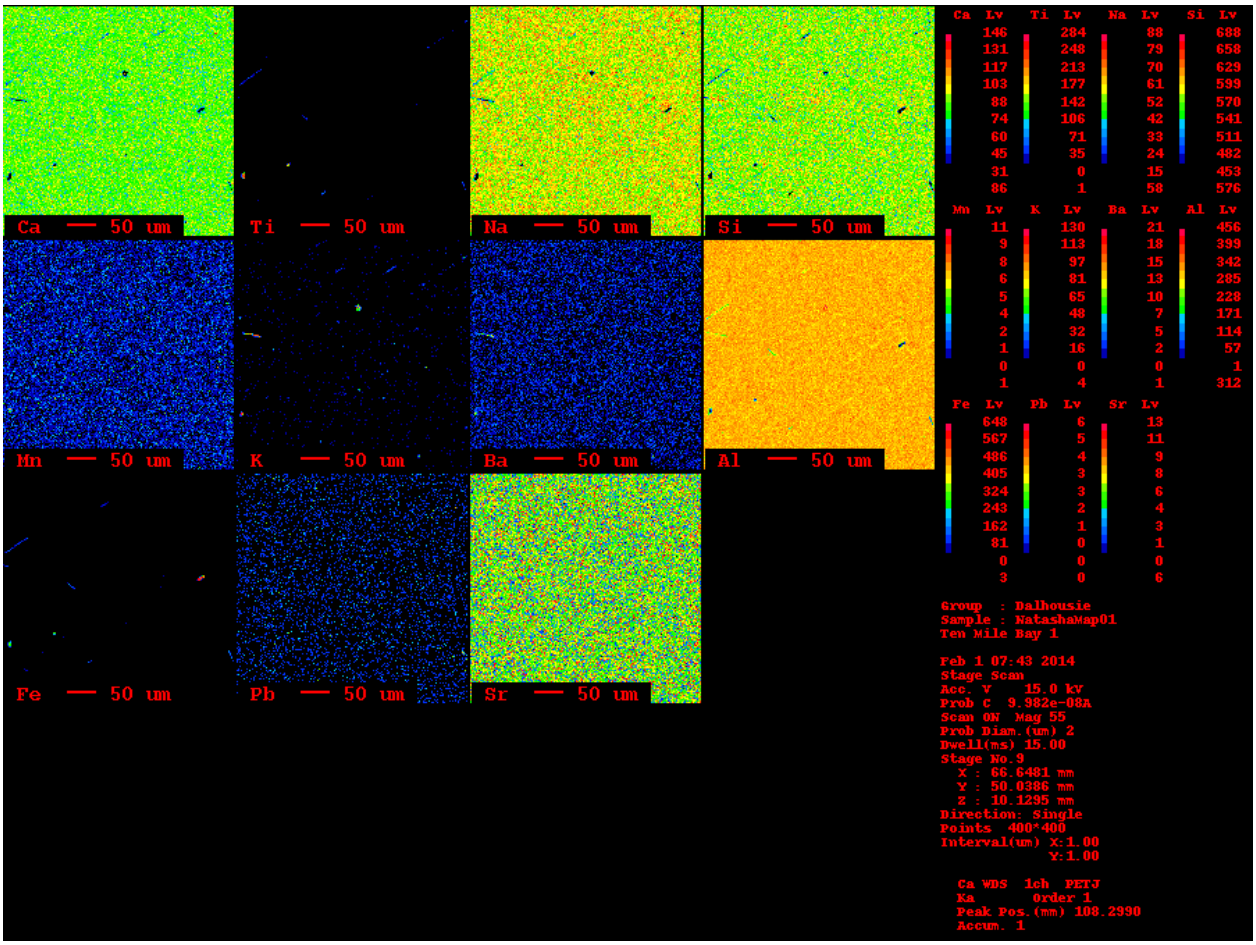

Ten Mile Bay-1 – Micro-exsolutions in Labradorite

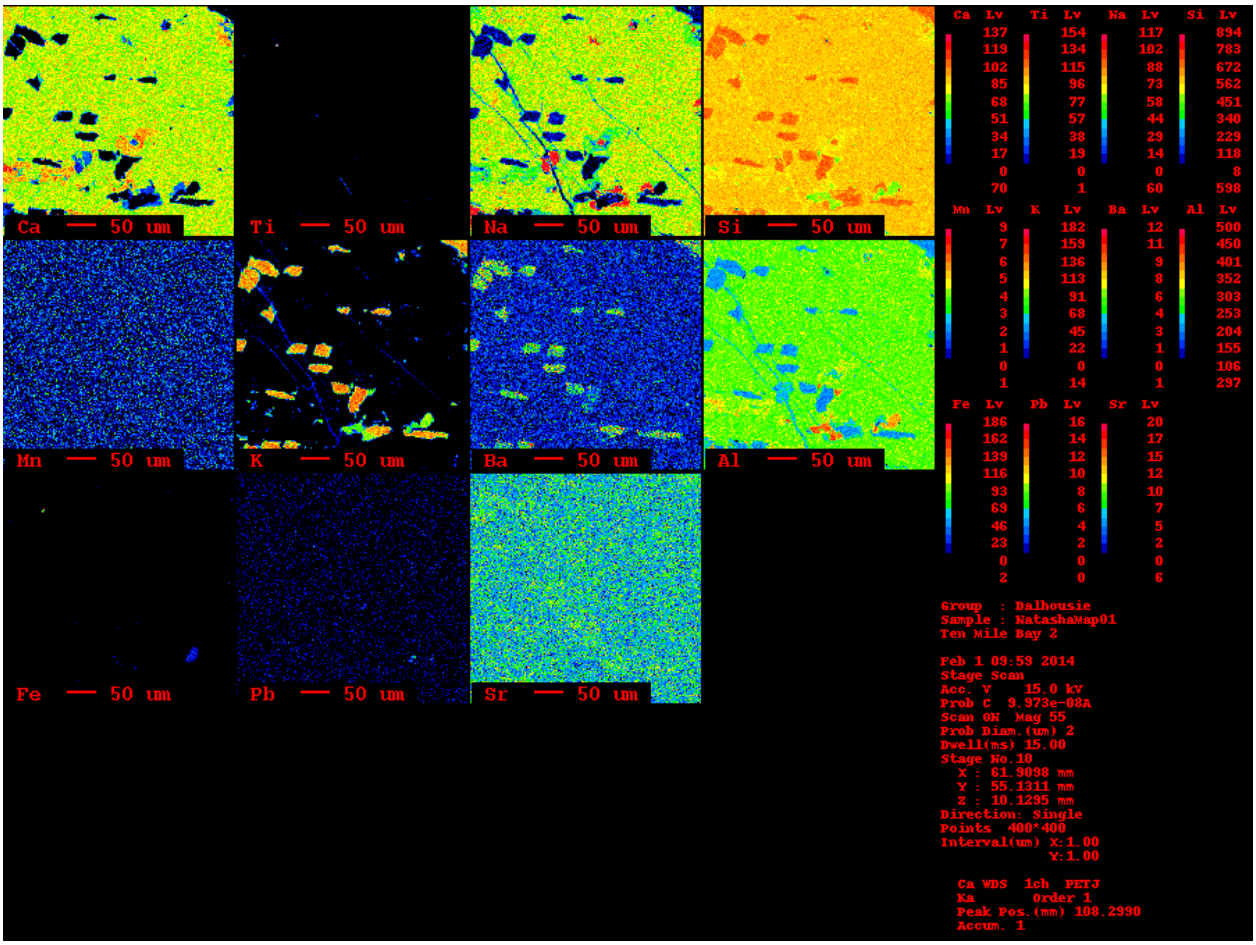

Ten Mile Bay-2 – Micro-exsolutions in Labradorite

APPENDIX D

	Microcline Exolution 1	Microcline Exolution 2	Microcline Exolution 3	Microcline Exolution 4	Microcline Exolution 5	Microcline Exolution 6	Microcline Body 1	Microcline Body 2	Microcline Body 3
SiO2	67.498	68.352	67.72	68.178	67.222	67.652	63.45	63.808	63.067
Al2O3	19.286	18.539	19.037	19.006	19.291	18.696	17.95	17.906	17.717
TiO2	0	0	0	0	0	0	0	0	0
FeO	0	0.037	0	0	0	0	0.016	0.036	0.014
MnO	0	0	0	0	0	0	0	0	0
CaO	0.483	0.75	0.309	0.152	0.426	0.019	0.034	0.032	0.032
Na2O	11.209	10.629	11.252	11.2	11.359	10.983	0.458	0.458	1.287
K2O	0.115	0.073	0.099	0.141	0.13	0.222	15.755	15.712	14.842
BaO	0	0	0	0	0	0	0	0	0
PbO	0	0	0	0	0	0.046	0.02	0.01	0
SrO	0	0.016	0.027	0	0.005	0	0	0	0
Total	98.591	98.396	98.444	98.677	98.433	97.618	97.683	97.962	96.959

	Microcline Body 4	Microcline Body 5	Microcline Edge 1	Microcline Edge 2	Microcline Edge 3	Microcline Edge 4	Microcline Edge 5	Orthoclase Exolution 1	Orthoclase Exolution 2
SiO2	63.276	63.307	67.003	63.534	62.927	67.273	63.209	67.746	67.222
Al2O3	17.769	17.826	18.528	17.752	17.641	19.103	17.793	19.381	19.294
TiO2	0	0	0	0	0	0	0	0	0
FeO	0.039	0.013	0	0.014	0.007	0	0.019	0.033	0
MnO	0	0	0	0	0	0	0	0	0
CaO	0.02	0.013	0.073	0.023	0.009	0.299	0.024	0.419	0.477
Na2O	0.499	0.336	7.833	0.918	0.302	11.249	0.704	11.401	11.311
K2O	15.801	16.143	5.368	15.55	15.851	0.129	15.501	0.167	0.067
BaO	0	0	0	0	0	0	0	0	0
PbO	0	0	0	0	0	0	0	0.029	0
SrO	0	0	0	0	0	0	0	0.01	0
Total	97.404	97.638	98.805	97.791	96.737	98.053	97.25	99.186	98.371

	Orthoclase Exolution 3	Orthoclase Exolution 4	Orthoclase Exolution 5	Orthoclase Body 1	Orthoclase Body 2	Orthoclase Body 3	Orthoclase Body 4	Orthoclase Body 5	Orthoclase Edge 1
SiO2	66.468	96.561	67.468	63.421	63.624	63.947	63.906	63.886	63.627
Al2O3	19.574	0.006	19.398	17.776	17.882	17.947	17.845	18.01	17.873
TiO2	0	0	0	0	0	0	0	0	0
FeO	0.018	0	0	0.044	0.018	0.047	0.023	0.035	0.003
MnO	0	0	0	0	0.007	0.015	0.006	0	0
CaO	0.86	0	0.404	0.02	0	0.008	0.027	0.012	0.025
Na2O	11.004	0.006	11.212	0.472	0.45	1.736	0.313	2.099	0.212
K2O	0.105	0.016	0.075	15.583	15.698	14.198	15.501	13.436	15.938
BaO	0	0	0	0	0	0	0	0	0
PbO	0.095	0.066	0.019	0.058	0.043	0.043	0.043	0.043	0.008
SrO	0.006	0.042	0	0	0	0	0	0	0
Total	98.13	96.697	98.576	97.374	97.722	97.941	97.664	97.521	97.686

	Orthoclase Edge 2	Orthoclase Edge 3	Orthoclase Edge 4	Orthoclase Edge 5	Orthoclase Micro 6	Labradorite 1	Labradorite 2	Labradorite 3	Labadorite 4
SiO2	67.263	63.589	67.677	67.018	67.549	51.162	51.761	51.017	52.285
Al2O3	19.279	17.781	18.831	18.581	18.919	29.538	28.841	29.805	29.03
TiO2	0	0	0	0	0	0	0	0	0
FeO	0.017	0.029	0.008	0.001	0.01	0.29	0.449	0.181	0.09
MnO	0	0.011	0	0	0	0	0	0	0
CaO	0.487	0.005	0.114	0.174	0.039	13.239	12.393	13.525	12.516
Na2O	10.3	0.498	9.916	8.346	11.433	4.296	4.573	3.997	4.649
K2O	0.373	15.685	1.323	4.435	0.161	0.251	0.541	0.227	0.159
BaO	0	0	0	0	0	0	0	0	0
PbO	0.096	0.048	0.07	0.039	0	0.038	0.043	0.048	0.038
SrO	0	0	0	0	0.093	0.031	0	0.054	0.023
Total	97.815	97.646	97.939	98.594	98.204	98.845	98.601	98.854	98.79

	Labradorite 5	Anorthite Micro 1	Anorthite Micro 2	Anorthite Micro 3	Anorthite Micro 4	Anorthite Micro 5	Anorthite Body 1	Anorthite Body 2	Anorthite Body 3
SiO2	52.521	62.447	62.179	61.711	62.056	62.455	54.77	53.2	54.277
Al2O3	28.247	18.215	18.083	18.111	18.171	18.148	26.711	27.236	27.343
TiO2	0	0	0	0	0	0	0	0	0
FeO	0.116	0.06	0.042	0.072	0.036	0.021	0.184	0.205	0.212
MnO	0.002	0	0	0.007	0.016	0	0	0	0
CaO	11.82	0.083	0.203	0.063	0.041	0.058	10.209	11.032	10.744
Na2O	4.794	0.486	0.516	0.599	0.567	0.669	5.737	5.327	5.413
K2O	0.468	15.093	15.067	14.842	14.774	15.029	0.382	0.289	0.359
BaO	0	1.246	1.383	1.544	1.551	1.183	0	0	0
PbO	0.078	0.078	0.013	0	0.061	0.031	0.086	0.026	0.026
SrO	0.052	0	0	0	0	0	0.029	0.036	0.058
Total	98.098	97.708	97.486	96.949	97.273	97.594	98.108	97.351	98.432

	Anorthite Body 4	Anorthite Body 5	Diorite 1	Diorite 2	Diorite 3	Diorite 4
SiO2	54.675	54.973	52.519	58.914	63.5	59.497
Al2O3	27.207	26.565	28.612	24.742	17.813	24.354
TiO2	0	0	0	0	0	0
FeO	0.202	0.198	0.122	0.088	0.066	0.159
MnO	0.01	0	0.008	0	0	0
CaO	10.709	10.168	12.309	7.19	0.014	6.8
Na2O	5.518	5.846	4.847	7.527	0.886	7.696
K2O	0.342	0.383	0.202	0.278	15.085	0.363
BaO	0	0	0	0	0	0
PbO	0.001	0.046	0	0.016	0.036	0.082
SrO	0.053	0.019	0	0	0	0
Total	98.717	98.198	98.619	98.755	97.4	98.951